Heavy-ion collisions at the LHC

G. Roland,[1] K. Šafařík,[2] P. Steinberg,[3]

[1]MIT, USA
[2]CERN, Geneva, Switzerland
[3]Brookhaven National Laboratory, Brookhaven, NY, USA

December 10, 2013

Abstract

1 Introduction

1.1 Physics motivation

1.2 LHC heavy-ion running

1.3 Detectors at the LHC

2 Event characterization

The first analyses of LHC heavy-ion data dealt with the charged particle density and the energy density achieved in Pb–Pb interactions at an unprecedent collision energy of $\sqrt{s_{\rm NN}} = 2.76$ TeV per nucleon pair in centre-of-mass system. The estimated values, as well as the results of practically all other measurements, strongly depend on the geometry of the collision (also called centrality), more precisely on the distance b of the centres of colliding nuclei in the plane transverse to the beam axis, called impact parameter of the collision. The impact parameter determines the volume of the interaction region, i.e. how violent the collision was. In this Section we first describe how the centrality of Pb–Pb collisions is determined, and then we turn to the basic measurements which characterize these interactions at the LHC.

2.1 Centrality determination

The lead nuclei are relatively extended objects, their size is about 14 fm across. To classify events according what part of the two nuclei participated in the interaction, the concept of collision centrality is commonly introduced in the field of heavy-ion physics. The centrality of the collision can be expressed in terms of geometrical parameters, such as the impact parameter b, or the number of participating nucleons. These parameters are inferred by comparison of experimental data with simulations of interactions. In this context the geometrical Glauber model is typically used [**?**], based on a description of

pA and A–A scattering, originally proposed by R.J. Glauber [**?**, **?**]. For the event simulation a Monte Carlo implementation of Glauber model is exploited [**?**, **?**], which is realized by the following steps:

- randomly sample the position of each nucleon inside the nucleus according to a Woods–Saxon distribution (two-parameter Fermi distribution), using the parameters extracted from the analysis of low-energy elastic e–A scattering [**?**];
- randomly sample the collision impact parameter b with probability distribution $P(b) \propto b\,\mathrm{d}b$ (up to $b_{\mathrm{max}} = 20$ fm, i.e. well above the lead nucleus diameter);
- assuming nucleons are moving along straight lines parallel to the beam direction, a pair of nucleons is considered as colliding if their centres are closer than $\sqrt{\sigma_{\mathrm{NN}}/\pi}$ in the transverse plane, where $\sigma_{\mathrm{NN}} = (64 \pm 5)$ mb is the inelastic nucleon–nucleon cross section, estimated from LHC pp measurements;

and for each event the number of nucleons participating in at least one collision (N_{part}) and the number of these binary collisions (N_{coll}) are counted. Then the total nuclear Pb–Pb cross section (σ_{PbPb}) is calculated as the fraction of πb_{max}^2 given by the ratio of the number of events with $N_{\mathrm{coll}} \geq 1$ to the number of all generated events. The cross section for collisions with impact parameter in the interval $(0, b)$ is obtained the same way, counting the events with $N_{\mathrm{coll}} \geq 1$ having the impact parameter within that interval. The centrality for this impact-parameter selection is its cross section expressed as the percentage of σ_{PbPb}. A centrality class is defined by its lower and upper percentages, corresponding to the events within impact-parameter interval $(b_{\mathrm{l}}, b_{\mathrm{u}})$, where the lower percentage is the part of σ_{PbPb} up to the impact parameter b_{l} and the upper percentage is that part up to b_{u}. Other characterizations of centrality classes, such as the mean number of participants $\langle N_{\mathrm{part}} \rangle$ and the mean number of binary collisions $\langle N_{\mathrm{coll}} \rangle$ (obtained as the average values for events within that class) are also employed. For completeness, the geometrical overlap function (integral of the convolution of the two transverse nuclear densities in the overlapping region) in the Monte Carlo formulation of Glauber model is defined as $T_{\mathrm{AA}} = N_{\mathrm{coll}}/\sigma_{\mathrm{NN}}$.

However, none of the geometrical quantities mentioned above (b, N_{part}, N_{coll}) is directly measurable in an experiment. Therefore, an experimental observable, which strongly correlates with the collision impact parameter, has to be used to classify the events according to their centrality. For example, the charged-particle multiplicity N_{ch} (or the energy deposition in a calorimeter) within a given pseudo-rapidity region is often used. The centrality selection of events within a certain impact-parameter interval is then replaced by a selection using a N_{ch} interval. In an ideal case, if one were able to measure the event distribution in such new selection variable for all Pb–Pb nuclear collisions, it would be possible to define centrality selection and centrality percentiles without any model, using only this distribution and its integral. However, for very peripheral collisions (large b, low N_{ch}) the experimental event sample is contaminated by electromagnetic interactions, at LHC energies these processes have a huge cross section (more than two orders of magnitude larger than the nuclear cross section) and contribute to low multiplicity events. It is necessary to suppress them, at least partly, already during the data taking (triggering on a minimum multiplicity value, or requiring some signal in ZDC's, see Sec. 1.3), which inevitably makes the event trigger less efficient for very peripheral collisions. For these reasons, the event distribution in a variable such as N_{ch} is usable for centrality selection only above some value, typically excluding peripheral collisions corresponding to the centrality class 90–100 %, where the contamination and the trigger inefficiency cannot be neglected. In order to determine the value, from which the distribution can be used, and to relate this so-called anchor point to the centrality, two approaches are utilized. The simulation of the Pb–Pb electromagnetic processes together with the experiment's trigger response gives the possibility to correct the event distribution of the selection variable, and to estimate a reasonable position of the anchor point with its centrality. Alternatively, the Glauber Monte Carlo

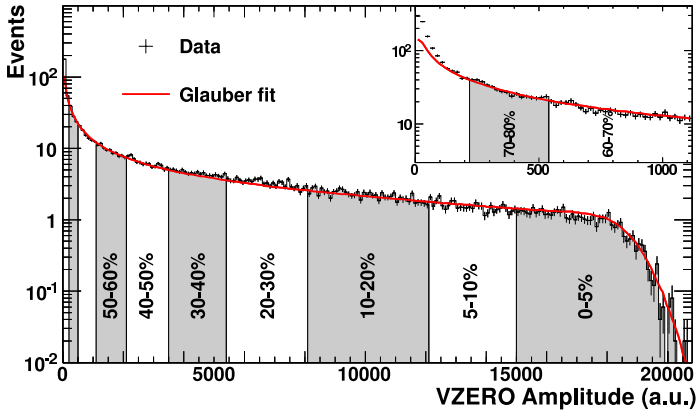

Figure 1: Distribution of the sum of amplitudes from the VZERO scintillators in the ALICE experiment (histogram) fitted to Glauber Monte Carlo coupled to NBD multiplicity production model (line). The inset shows peripheral-collision region enlarged. Reproduced from [**?**].

can be supplemented with a model of particle production, describing the experimental selection-variable distribution and finding the point where the two deviate. Such an approach also allows to calculate for a given centrality selection the corresponding $\langle N_{\rm part}\rangle$ and $\langle N_{\rm coll}\rangle$, taking into account the finite resolution of the selection variable $N_{\rm ch}$ with respect to the collision impact parameter b.

A simple model for multiplicity production, exploited together with a Glauber Monte Carlo, consists in the simulation of the multiplicity distribution from one particle source and a prescription for the number of particle sources depending on the collision geometry, called the number of ancestors ($N_{\rm anc}$). For the multiplicity distribution the Negative Binomial Distribution (NBD) is typically used, it has two parameters (controlling the mean and width), and describes reasonably well the charged-particle multiplicity in different pseudo-rapidity windows for high-energy pp interactions. The number of particle sources is parameterized as a function of $N_{\rm part}$ and $N_{\rm coll}$, the common choice being $N_{\rm anc} = fN_{\rm part} + (1-f)N_{\rm coll}$, motivated by a two-component model, where the number of sources is composed of soft (proportional to $N_{\rm part}$) and hard (proportional to $N_{\rm coll}$) interactions. Thus, such a model has three parameters, two for the NBD and f for $N_{\rm anc}$, which are fitted to the experimental distribution of the selection variable between the anchor point and the maximal value (most central collisions).

Figure 1 illustrates the result of such a fit to the event distribution of the sum of amplitudes from the VZERO counters (cf. Sec. 1.3) in the ALICE detector. This variable is proportional to the multiplicity in the pseudo-rapidity region covered by the VZERO detector. The centrality classes and their percentiles are determined by integrating the experimental distribution from its maximal value down to the anchor point. Simulated events are then used to calculate $\langle N_{\rm part}\rangle$ and $\langle N_{\rm coll}\rangle$ for the centrality classes. The ATLAS experiment for the centrality selection is using transverse energy measured in Forward Calorimeters (FCal), and the CMS experiment bases its Pb–Pb centrality selection on Hadron Forward (HF) calorimeter, covering a similar pseudo-rapidity region. Another detector commonly used for centrality measurements is the ZDC. Its disadvantage is that, unlike for the multiplicity-type detectors, the ZDC response is not a monotonic function of centrality: it gives small signals both for very central and for very peripheral collisions. ZDC's are therefore normally used in correlation with some other detector, especially for central and very central events.

The centrality determination and its uncertainties affect practically all the results from the analyses of heavy-ion data. A careful systematic study of the centrality selection dependence on different assumptions is always required. This usually includes: variation of the parameters describing the nucleus density; including or not a minimal separation between nucleons inside each nucleus; modifying the definition of colliding nucleons (from a black-disc assumption to a Gaussian profile description, or introducing an intra-nuclear rescattering); and changing the functional dependence of $N_{\rm anc}$, if used, to

a power function of $N_{\rm part}$ or $N_{\rm coll}$. All these uncertainties must then be properly propagated to the measurements of other quantities.

2.2 Charged-particle density

Traditionally, the very first measurements of heavy-ion collisions at a new energy regime comprise the charged-particle density, and its centrality dependence. These measurements were performed by all three experiments participating in the LHC heavy-ion programme, and the first results were published already during the first heavy-ion run [**?**]. The methods exploited to measure the charged-particle density ($\mathrm{d}N_{\rm ch}/\mathrm{d}\eta$) in the mid-rapidity region ($|\eta| < 0.5$) were very similar. All experiments used their silicon pixel trackers, detectors closest to the interaction point, to count so called tracklets — pairs of reconstructed hits (pixel clusters) in two layers of the pixel detectors aligned with the primary vertex. Other methods, such as measuring the cluster multiplicity, partial tracking with innermost detectors, and TPC tracking (in the case of ALICE), were also utilized. The collision-energy dependence of $\mathrm{d}N_{\rm ch}/\mathrm{d}\eta$ for the most central heavy-ion collisions, normalized per participant pair (i.e. $\langle N_{\rm part}\rangle/2$), is presented in Fig. 2, top part. The results from the three experiments are in excellent agreement, and they show an increase by more than factor of two, compared to the highest value observed at RHIC. The energy dependence of the charged-particle density can be satisfactorily parameterized by a power function: $\propto s_{\rm NN}^{0.15}$. Note that the energy dependence for heavy ions is significantly steeper than that for pp interactions ($\propto s^{0.11}$), this is also reflected by the more than a factor two higher value of the normalized charged-particle density $(\mathrm{d}N_{\rm ch}/\mathrm{d}\eta)/(0.5\langle N_{\rm part}\rangle$ in heavy-ion collisions compared to pp interactions. It is interesting to note that most of the theoretical and model predictions for the LHC charged-particle density underestimated the experimental observation, contrary to a clear tendency for an overestimation when the first results from RHIC experiments were published.

In the bottom part of Fig. 2 the centrality dependence of the same quantity $(\mathrm{d}N_{\rm ch}/\mathrm{d}\eta)/(0.5\langle N_{\rm part}\rangle$, expressed as a function of $\langle N_{\rm part}\rangle$, is presented. Again, very good agreement among the three LHC experiments is observed. The data from RHIC (average value over the four experiments) are also shown, multiplied by a factor 2.15 to match the points for the most central collisions. The normalized charged-particle density is rising with centrality, which means that the particle multiplicity at mid-rapidity increases faster than the number of participants, presumably due to the contribution of hard processes to the multiplicity production. However, this increase is very similar to that observed at the top RHIC energy. Apart from a simple interpretation of these data in terms of (a mixture of) soft and hard interactions, model calculations implementing a saturation picture, where the number of soft gluons available for the multiplicity production is progressively reduced by parton recombination, attempt to determine the energy and centrality dependence of the saturation scale.

The experiments were also looking for the $\mathrm{d}N_{\rm ch}/\mathrm{d}\eta$ evolution in the longitudinal direction, i.e. as a function of pseudo-rapidity. The ATLAS collaboration published the charged-particle densities for different centrality classes in $|\eta| < 2$ [], and the CMS detector measured $\mathrm{d}N_{\rm ch}/\mathrm{d}\eta$ in the interval $|\eta| < 2.5$ []. The ALICE experiment extended the pseudo-rapidity coverage of such measurement to $-5 < \eta < 5.5$, exploiting the FMD (cf. Sec. 1.3) and so called satellite bunches. The latter are created in the accelerator RF cavities, when a small fraction of particles slips from the main bunch into another wave period, 75 cm apart (corresponding to RF frequency 400 MHz). This way, very low-intensity satellite collisions, distanced by every 37.5 cm from the main bunch crossing, are produced, shifting the pseudo-rapidity acceptance. Figure 3 shows the results of the ALICE pseudo-rapidity distribution measurement, compared to the data previously obtained by CMS and ATLAS. The wide-rapidity data are used together with the RHIC results (from the BRAHMS and PHOBOS experiments) to confirm limiting fragmentation — the shape of the distributions are in the fragmentation region independent of the collision energy. By extrapolation, the total charged-particle multiplicity in Pb–Pb collisions at $\sqrt{s_{\rm NN}} = 2.76$ TeV for different centralities can be estimated, for example, in 5 % of the most central

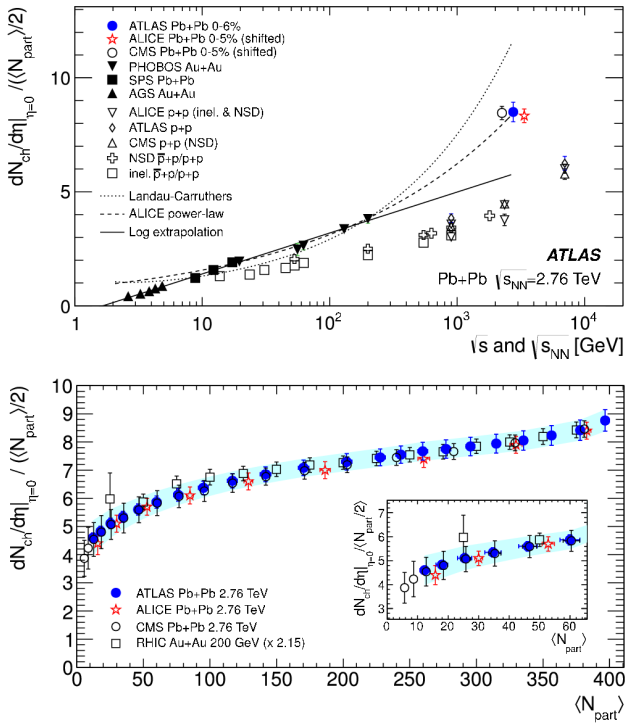

Figure 2: Top: Energy dependence of the charged-particle density at mid-rapidity ($|\eta| < 0.5$) normalized per participant nucleon pair, from various pp (and $\overline{\mathrm{p}}$p) measurements, and most central heavy-ion collisions. The curves represent various extrapolations from lower-energy data to LHC, the one describing heavy-ion experimental points (dashed line) is a power function $(\mathrm{d}N_{\mathrm{ch}}/\mathrm{d}\eta)/(0.5\langle N_{\mathrm{part}}\rangle) \propto s_{\mathrm{NN}}^{0.15}$ proposed in [**?**]. Bottom: $\langle N_{\mathrm{part}}\rangle$ dependence of the charged-particle density normalized per participant nucleon pair from the three LHC experiments, compared to average value from RHIC experiments, multiplied by a factor 2.15. The inset shows in detail the peripheral-collision region with $\langle N_{\mathrm{part}}\rangle < 60$. Reproduced from [**?**].

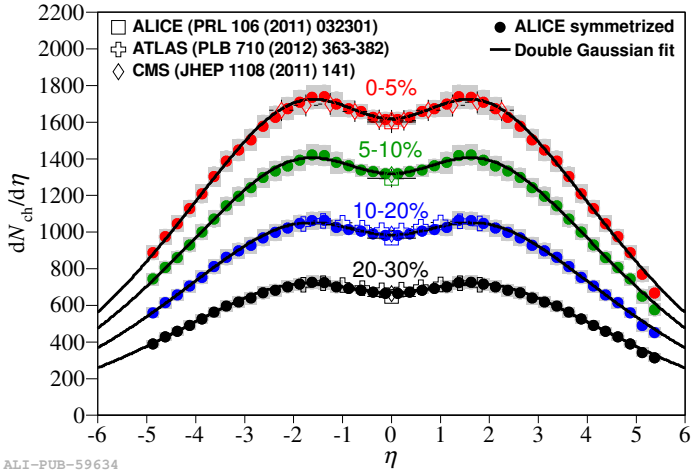

Figure 3: Charged-particle pseudo-rapidity density distribution for various centrality classes, comparison among the LHC experiments. Reproduced from [].

events $(17.2 \pm 0.8) \times 10^3$ charged particles are created.

2.3 Energy density

In order to estimate the energy density achieved in Pb–Pb collisions at the LHC, the measurements of the transverse energy pseudo-rapidity density, $\mathrm{d}E_\mathrm{T}/\mathrm{d}\eta$ were performed. The CMS experiment measured directly the energy flow in calorimeters for different pseudo-rapidities and centralities [**?**]. The collision energy dependence of $\mathrm{d}E_\mathrm{T}/\mathrm{d}\eta$ at mid-rapidity for the most central heavy-ion collisions, normalized to the the number of participant pairs, is shown in Fig. 4. An increase by more than a factor three is observed from the top RHIC energy to the LHC. This collision-energy dependence can be satisfactorily described by a power function $\propto s_\mathrm{NN}^{0.2}$, which means that the transverse-energy density rises with collision energy faster than the particle density, indicating a significant increase of the average transverse momentum of particles produced in the LHC heavy-ion interactions. The ALICE experiment confirmed the CMS results estimating $\mathrm{d}E_\mathrm{T}/\mathrm{d}\eta$ from $\mathrm{d}N_\mathrm{ch}/\mathrm{d}\eta$ and the measured transverse-momentum spectra for different hadron species.

Even in forward region, up to $|\eta| = 5$, the transverse-energy density observed at the LHC is larger than that at mid-rapidity at the top RHIC energy. The energy density achieved in heavy-ion interactions (ϵ) is commonly related to the transverse-energy density by the Bjorken formula [], based on geometrical considerations. It can be expressed as $\epsilon\tau_0 = (\mathrm{d}E_\mathrm{T}/\mathrm{d}y)/S$, where τ_0 denotes the time when the initial thermalization was established (supposed to be $\tau_0 \leq 1$ fm), and S is the transverse overlap area, approximated for central Pb–Pb collisions with $\pi(7\,\mathrm{fm})^2$. For the top 5 % centrality CMS obtained $\epsilon\tau_0 = 14$ GeV/fm^2 (using a model estimation for Jacobian $\mathrm{d}\eta/\mathrm{d}y \approx 1.1$). This represents a factor 2.6 increase with respect to the highest RHIC collision energy, and an even larger increase for the energy density ϵ, since the time τ_0 is expected to be shorter at the LHC.

3 Particle spectra and yields

3.1 Charged-particle transverse momentum spectra

Transverse momentum spectra of charged particles were measured by all three experiments exploiting the first collected data sample. They are presented as the dependence of the (inclusive) invariant cross section on the transverse momentum (p_T), and finally in the form normalized to pp measurement at the

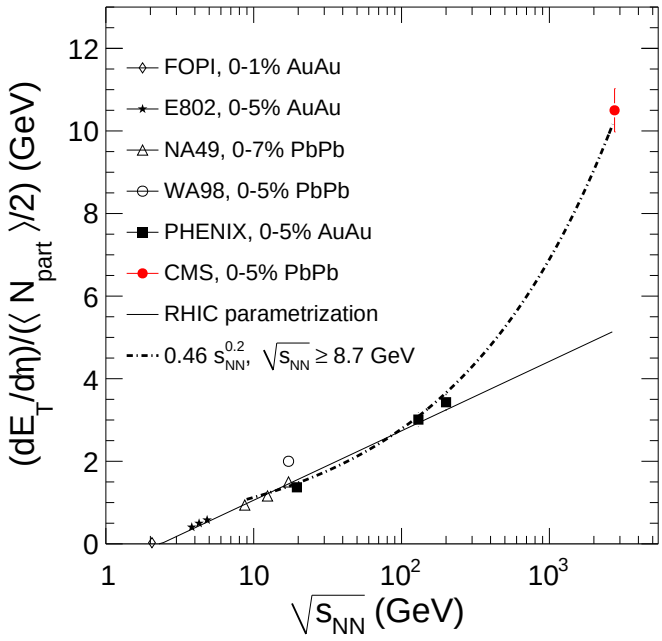

Figure 4: Collision energy dependence of the transverse-energy pseudo-rapidity density at mid-rapidity, normalized to the number of participant pairs, for central heavy-ion collisions. The curves represent various extrapolations from lower-energy data to LHC, the one describing the LHC measurement (dashed–dotted line) is a power function $(\mathrm{d}E_\mathrm{T}/\mathrm{d}\eta)/(0.5\langle N_\mathrm{part}\rangle) \propto s_\mathrm{NN}^{0.2}$ proposed in [**?**], from where this figure is reproduced.

same nucleon–nucleon energy. For the latter representation, the nuclear modification factor is defined as

$$R_\mathrm{AA}(p_\mathrm{T}) = \frac{\mathrm{d}N_\mathrm{ch}^\mathrm{AA}(p_\mathrm{T})/\mathrm{d}p_\mathrm{T}}{\langle N_\mathrm{coll}\rangle\, \mathrm{d}N_\mathrm{ch}^\mathrm{pp}(p_\mathrm{T})/\mathrm{d}p_\mathrm{T}}, \tag{1}$$

where on the right hand side the superscripts AA and pp refer to the values obtained in heavy-ion and pp measurements, respectively. If a collision of two nuclei behaved as a simple superposition of N_coll nucleon–nucleon collisions, the nuclear modification factor would be $R_\mathrm{AA} = 1$. Such a scaling with the number of binary collision N_coll is a natural expectation for hard processes, in case that nucleons act independently and their interactions are not influenced by the rest of the nuclei. A deviation of R_AA from unity for hard processes signals a nuclear effect. However, for soft processes, such as particle production at p_T below a few GeV, the scaling from pp to AA is governed by N_part rather than by N_coll leading to a higher R_AA in that p_T region, especially for central events.

The p_T spectrum for charged particles in LHC heavy-ion collisions was expected to be suppressed at high p_T with respect to pp interactions. The fact that R_AA is significantly below unity at p_T above a few GeV was well established for central collisions at RHIC, and attributed to the jet quenching — an energy loss of hard partons in their interactions with the surrounding high-density nuclear matter. As the high p_T particles are supposed to be produced in the fragmentation of such hard partons, their quenching lowers the particle production, reflecting the amount of energy loss, and thus the density of nuclear matter created in the collision. However, the value of R_AA is also dependent on the steepness of the parton p_T spectrum (a harder parton spectrum at the LHC should result in less particle suppression), and on the nuclear modification of the structure functions (distribution of partons inside a nucleon). Therefore, for theoretical predictions and interpretations of the R_AA behaviour, model calculations taking into account the interplay of many effects are necessary.

The first LHC measurement of charged-particle R_AA, was published by ALICE, presenting the p_T

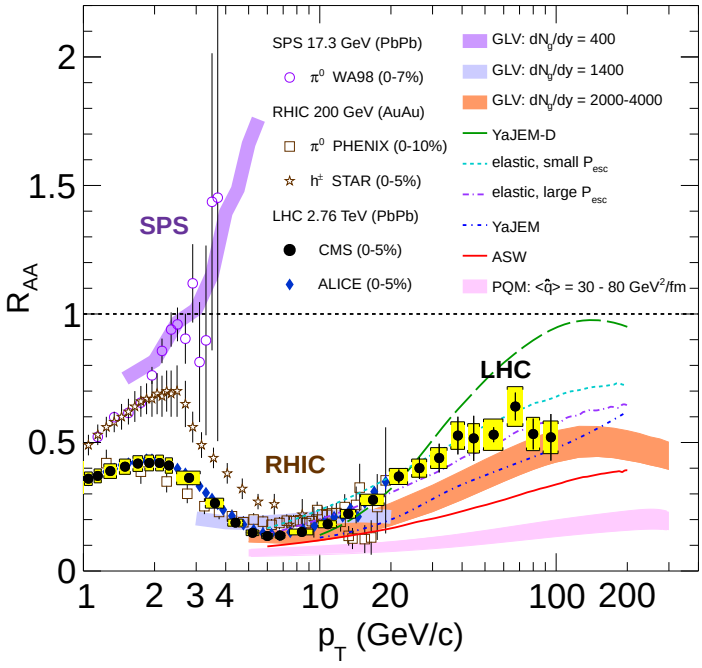

Figure 5: Transverse momentum dependence of nuclear modification factor $R_{\rm AA}$ for charged particles produced in central heavy-ion collisions at LHC and lower energies. The curves and bands represent different model calculations. Reproduced from [].

spectrum up to 20 GeV, for the 5 % most central Pb–Pb events. It showed a slightly stronger suppression compared to RHIC: the largest suppression — in the $p_{\rm T}$ range 6–7 GeV — was a factor about 7 at the LHC, while at RHIC a factor of 5 was observed. A new observation was that with increasing $p_{\rm T}$ the suppression gets smaller, i.e. $R_{\rm AA}$ increases. This was soon confirmed by the CMS measurement [], extending the $p_{\rm T}$ reach up to 100 GeV (see Fig. 5). The nuclear modification factor $R_{\rm AA}$ exhibits a clear increase up to $p_{\rm T}$ about 40 GeV, and and then seems to saturate with the $R_{\rm AA}$ value about 0.5–0.6 for the most central collisions. Figure 5 also shows the $p_{\rm T}$ dependence of $R_{\rm AA}$ at lower energies, and a variety of model calculations. Different models can be tuned to fairly reproduce the $R_{\rm AA}$ data, however, it remains to demonstrate that they describe with the same parameters the ensemble of other observables, especially the azimuthal anisotropy (Sec. 5).

The ALICE and CMS experiments also measured the $R_{\rm AA}$ $p_{\rm T}$ dependence for different collision centralities. The charged-particle production is, as expected, less and less suppressed as one moves from central to peripheral Pb–Pb collisons. The ATLAS collaboration reported similar results, presented as $R_{\rm CP}$ as a function of $p_{\rm T}$, where $R_{\rm CP}$ stands for a quantity analogue to that defined in Eq. 1 using the normalized ratio of heavy-ion results at different centralities (the subscript CP indicates the central-to-peripheral ratio), commonly using the most peripheral class available for normalization.

3.2 Identified-hadron spectra

Study of the particle composition as a function of $p_{\rm T}$ reveals a mass hierarchy, interpreted as resulting from a common radial-velocity field created during the expansion of the dense-matter fireball. Such a collective flow arises in strongly interacting matter in the presence of a pressure gradient. Having the same velocity, heavier particles (e.g. protons) will acquire a larger momentum than lighter mesons. This effect is clearly visible in Fig. 6, where the $p_{\rm T}$ spectra for pions, kaons, and protons measured by the ALICE experiment [] exploiting various particle-identification techniques, are presented for the top 5 % central events. From the simultaneous blast-wave fit to these spectra (excluding pions with

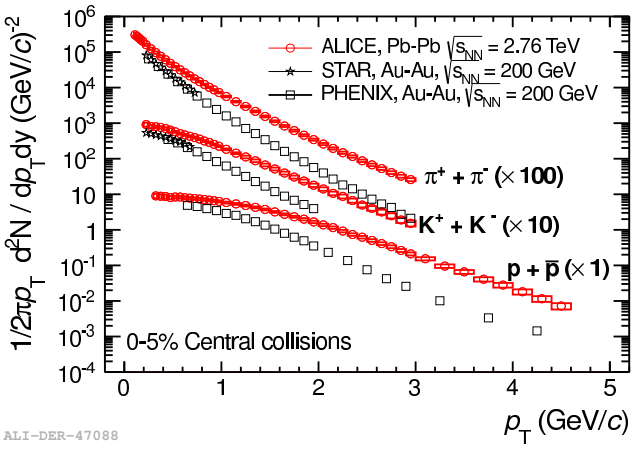

Figure 6: Transverse momentum spectra for pions, kaons, and protons (sum of particles and antiparticles) produced in 5 % of most central Pb–Pb collisions at LHC, compared to the RHIC measurements. Reproduced from [].

$p_{\rm T} < 0.5$ GeV and kaons with $p_{\rm T} < 0.35$ GeV where resonance decays largely contribute), the kinetic freeze-out temperature ($T_{\rm kin}$, temperature when the hadrons cease to interact) and an average radial velocity ($\langle\beta\rangle$) is estimated. The two parameters were extracted for different centralities, and they were found to be strongly correlated, since they both determine the slope of the $p_{\rm T}$ spectra. Both $T_{\rm kin}$ and $\langle\beta\rangle$ are higher compared to RHIC, and they depend on centrality: $T_{\rm kin}$ being lower for more central collisions, while $\langle\beta\rangle$ increases. The values reached for 5 % of most central collisions are $T_{\rm kin} \approx 95$ MeV and $\langle\beta\rangle \approx 0.65$, the latter being more than 10 % above the RHIC value. These spectra were compared further to various hydrodynamical-model calculations [], and a fair description for the bulk production, up to transverse momenta 2–3 GeV, i.e. where such models are applicable, is observed for central collisions. In some cases [] the agreement is improved by supplementing the hydrodynamical calculations with a hadronic rescattering code (UrQMD [], in this occasion). But going to more peripheral collisions the hydrodynamical description becomes worse.

The $p_{\rm T}$ spectra of identified charged hadrons are determined up to $p_{\rm T} = 20$ GeV, exploiting the measurement of ionization energy losses in the ALICE TPC in the relativistic rise region. Figure **??** presents these results normalized to the pp baseline, as $R_{\rm AA}$ for pions, kaons, and protons, compared to the (averaged) charged-particle data. It is clearly seen that for $p_{\rm T}$ above 7–8 GeV the behaviour for all particle species coincides. For lower $p_{\rm T}$ a mass hierarchy appears: the heavier the particle, the lower its suppression. These observations suggest the presence of three regions in transverse momentum:

- bulk region, low $p_{\rm T}$ up to 2–3 GeV, where the production comes from the hadronization of high-density strongly-interacting matter created in a heavy-ion collision, reflecting collective radial flow, fairly described (at least for central collisions) by hydrodynamical models;

- intermediate region, in $p_{\rm T}$ up to 7–8 GeV, where still a mass splitting among various particle species persists that can be attributed a reminiscence of radial flow (the difference has to disappear for $p_{\rm T}$ values significantly larger than particle masses), however, additional ideas were put forward to push further in $p_{\rm T}$ this mass distinction, such as constituent-quark recombination which would favour baryons to acquire larger $p_{\rm T}$ than mesons;

- fragmentation region, above 7–8 GeV in $p_{\rm T}$, where the different hadron species exhibit a common suppression pattern, and consequently their relative abundances are the same as in pp collisions, naturally explained as being fragmentation products of a high-$p_{\rm T}$ parton coming from a hard scattering at early stage (which itself is quenched by the surrounding high-density matter).

To look in detail into the intermediate region, it is instructive to plot the proton-to-pion ratio as a function of p_{T}, fig. **??**. The striking effect is that for central collisions at p_{T} around 2.5–3 GeV this ratio is more than a factor three higher than the value for pp collisions. This so-called baryon anomaly was observed already at RHIC, and certainly the low-p_{T} rise is explained by the hydrodynamical radial flow. In the intermediate region, where the hydrodynamics ceases to work, the behaviour is qualitatively described by models involving constituent-quark recombination or baryon string-junction transfer along the axis of a fragmenting jet. These models, however, tend to predict an anomalous baryon-to-meson ratio even for significantly higher p_{T} than actually observed. On the other hand, a smooth connection between the hydro-described bulk region and the normal-ratio fragmentation region, using a realistic radial-flow profile, will probably move the border between the intermediate and fragmentation regions to lower than observed values. Therefore, a comprehensive description of the particle production in the intermediate region is still an open, and experiment driven issue.

3.3 Strange-particle production

Historically, the enhancement of strangeness production was among the first signatures proposed to signal a qualitatively different state of matter, expected to be created in ultra-relativistic heavy-ion collisions []. The strangeness increase in high-temperature QCD matter is motivated by two reasons: the relevant quark masses drop from their constituent to their bare values, and then the strange-quark mass becomes comparable to the temperature, consequently the production rates for different light quarks tend to equalize. Strangeness enhancement was already observed at lower energies, at the SPS [], as well as at RHIC []. The systematic study of strangeness production at the LHC is under way in ALICE. In addition to charged kaons, the measurements include topologically identified particles ($\mathrm{K}^0_{\mathrm{s}}$, Λ, Ξ^-, and Ω^-), and resonances containing strangeness.

The enhancement of strangeness production is confirmed at the LHC, see Fig. **??**, albeit the enhancement factor, expressed as the ratio of the yield per participant in A–A collisions to that in pp (or pA) collisions, decreases slowly with the collision energy. This reflects the fact that the production of strange particles per pion in heavy-ion collisions practically saturates as $\sqrt{s_{\mathrm{NN}}}$ reaches few tens of GeV, while in pp it still increases from RHIC to the LHC, and only at the highest energy ($\sqrt{s}$ = 7 TeV) seems to cease its growth.

The strange-particle R_{AA} is also influenced by strangeness enhancement, especially in the bulk and intermediate p_{T} regions. As already mentioned, kaons, including $\mathrm{K}^0_{\mathrm{s}}$, are above the pion curve. The strange baryons have larger R_{AA} than protons, and R_{AA} increases with the strangeness content, exceeding unity for Ω^-. With increasing p_{T}, the strangeness R_{AA} goes progressively closer to the common fragmentation behaviour for all other particle species, still being for Ω^- at $p_{\mathrm{T}} \approx 7$ GeV above the others. These measurements are at this point limited by the available statistics.

Baryon-to-meson ratio in the strangeness sector is very similar to that of proton-to-pion. The Λ-to-$\mathrm{K}^0_{\mathrm{s}}$ ratio as a function of p_{T} is shown in Fig. **??** together with hydrodynamical- and recombination-model calculations. The EPOS model [], which includes the hydrodynamical expansion and, at higher p_{T}, the (mini-)jet fragmentation with an interaction between jets, describes the experimental measurement fairly well.

3.4 Resonance and light-nuclei production

The resonances are interesting to study in heavy-ion collisions, because of their short lifetime they may decay inside the medium, before the kinetic freeze-out. If a decay product scatter changing its momentum, the parent resonance cannot be observed by invariant-mass reconstruction, and that leads to an apparent depletion of the resonance yield, which is dependent on the resonance lifetime. On the other hand, resonances can be also recreated during the elastic scattering phase having a large

cross-section for s-channel production at very low energies. Therefore, the comparison of the different-lifetime-resonance yields with hadronic-transport models gives valuable information about the time evolution during the late stage of heavy-ion collisions.

At the LHC, the ALICE collaboration reported the measurements of $K^*(892)^0$ and ϕ mesons. The yield of K^{*0} relative to other particles (e.g. K^-) decreases significantly for more central collisions, while the ϕ yield normalized in the same way is compatible with being independent of centrality. This is qualitatively understood by an order of magnitude different lifetimes for the two resonances (4.2 fm and 46 fm for K^{*0} and ϕ, respectively). A substantially lower production of K^{*0} in central collisions also means that the regeneration is not effective enough to compensate the decay rate. Similar observations were made at RHIC []. The ϕ meson, being relatively long-lived to be treated as stable on the time scale of the heavy-ion collision, is of special interest. Its mass is close to that of the lightest baryons, therefore, the ϕ $p_{\rm T}$ spectrum can differentiate mass-dependent effects and constituent-quark-number effects. Preliminary data indicates compatibility between proton and ϕ $p_{\rm T}$ spectra up to 5 GeV, favouring thus the radial-flow explanation of the baryon anomaly to the constituent-quark-recombination one.

The high density of particles produced in heavy-ion collisions implies substantial rates for light-nucleus and hypernucleus production. The interest of such measurement is to study the production mechanism of such state, their coalescence coefficients, and their thermodynamical equilibrium with other particles. The light nuclei, such as d, t, ^{3}He, and ^{4}He, and corresponding antinuclei, were observed in heavy-ion collisions at RHIC and the LHC, and quantitative results for d and ^{3}He were reported by ALICE. These measurements use the particle identification based on the specific ionization losses in TPC and the TOF measurement. The production of hypernuclei (nuclei containing one ore more strange baryons) is of additional interests since the (unknown) properties of hypernuclei, their masses and decays, can be measured. The ALICE collaboration reconstructed the ${}^3_\Lambda{\rm H} \rightarrow {}^3{\rm He} + \pi^-$ decays, as well as the charge-conjugated ones, opening the study in this field at the LHC, following the first antihypertriton measurement at RHIC []. Searches for more exotic states, such as the H-dibaryon ($\Lambda\overline{\Lambda}$ bound state or six-quark state), the $\overline{\Lambda}\overline{\rm n}$ bound state, and the $\Phi(1860)$ pentaquark have not given any positive signal.

3.5 Particle yields

The particle yields at mid-rapidity are obtained by integration of the transverse-momentum spectra fitted to the blast-wave functional dependence (or other suitable function), in order to extrapolate below the lowest measured $p_{\rm T}$. Traditionally, the particle yields in heavy-ion collisions are studied within statistical hadronization models. These models are based on the grand-canonical ensemble, describing the system with the temperature ($T_{\rm ch}$), the baryon chemical potential ($\mu_{\rm b}$), and the volume in thermal and chemical equilibrium with the rest. Knowing these parameters it is straightforward to calculate the average number of various particles in the system. All the resonance and other unstable states, summed-up in the grand potential (usually with an upper mass cut-off about 2 GeV, as above the resonance spectrum is not well known), are decayed into observed particles and compared to the measurements. The temperature $T_{\rm ch}$ is interpreted as the chemical freeze-out temperature, below which the energy of hadronic re-scattering is lower than the threshold for inelastic interactions, and thus the particle composition remains unchanged.

The statistical models were used to describe the heavy-ion collision data from very low energies up to RHIC with a good agreement for most of the particle species. The temperature $T_{\rm ch}$ practically does not change with the collision energy, therefore, a reasonable estimate for LHC is the value observed at RHIC, $T_{\rm ch} = 164$ MeV; the chemical potential has to be very low as the ratio particles to antiparticles is for all species compatible with unity; $\mu_{\rm b} = 1$ MeV is usually assumed. The predictions using these parameter values are compared in Fig. **??** with the measurements of yield ratios: p/π and K/π, for

different centralities (expressed by particle density). The conclusion is that the measured proton yield for central Pb–Pb collisions at the LHC is by a factor of about 1.5 lower than predicted. In order to describe the proton measurement, significantly lower $T_{\rm ch}$ is needed (about 152 MeV), but then the yields of multi-strange baryons are underestimated. Trying to fit the temperature to the available data gives an estimate of $T_{\rm ch} \approx 156$ MeV, however, the fit description is not as good as it was at lower energies. Moreover, it is hard to expect that the chemical freeze-out temperature would decrease at higher energy.

It Seems that such problems were there partly already at RHIC. The discrepancy being smaller, and uncertainties in proton-yield corrections, lead to the fact that it was considered not significant. There are few attempts to explain the lower proton yield at the LHC:

- The baryons can annihilate in re-scattering with antibaryons, even after chemical freeze-out. This will affect protons more then strange baryons, because protons have larger density, and the annihilations with a strange partner are penalized due to presence of kaon(s) in final state, which shrink the phase space and thus lower the cross section of such cross-flavour annihilation. The effect was confirmed with UrQMD calculations [], and the particle density makes it larger at the LHC than at RHIC. It was also shown that multi-meson interactions, recreating the baryon–antibaryon pairs, are not, at decreasing temperature, effective enough to compensate the loss [].

- The statistical hadronization model assumes strictly the same $T_{\rm ch}$ for all particles, which may not necessarily be true. Motivated by recent lattice QCD calculations, flavour- and mass-dependent prehadronic states in QGP may alter the effective phase-transition temperature resulting in an non-uniform freeze out. This will consequently modify the yields predicted by the model.

- The high-mass resonances, not accounted for in the model, would presumably increase mostly the pion yield. Because of the number of these resonances can raise exponentially with the mass [**?**], even their production being exponentially dumped, the effect may be non-negligible. This would lower the $\rm p/\pi$ model prediction [**?**].

- The statistical hadronization model can be modified, incorporating non-equilibrium effects. In fact the model was used also to describe particle yields in pp, and even in $\rm e^+e^-$, interactions, however, an additional parameter suppressing strangeness production had to be used. Introducing two parameters regulating the population of phase space, separately for light-quarks and strange quark, allows for good description of the experimental measurements.

The lower-than-expected proton yield observed at the LHC was one of the first surprises from the heavy-ion programme, and its origin has yet to be established.

4 Non-flow correlations

4.1 Femtoscopic correlations

4.2 Charged particle rapidity correlations

4.3 Angular correlations

5 Flow correlations

5.1 Introduction

While the previous section covered physical mechanisms which induce correlations between multiple hadrons, this section covers the phenomenon of "collective flow", which leads to the correlations of

essentially all the particles in every event. This results from the translation of anisotropies in the initial shape of the colliding nuclei into anisotropies in momentum space, something that would not occur if individual nucleon-nucleon collisions emitted independently of each other. The characterization of a "shape" in a final state particle distribution is typically performed using a Fourier decomposition of the azimuthual angle distrbution of final state particles. Of course, averaging over an ensemble of independent events would lead to the observation of no net anisotropy. Thus, the presence of harmonic oscillations in the final state requires the estimation of an "event plane" from the particle themselves, with an axis that points in the direction of the largest momentum flow.

While this phenomenon was observed decades ago in the collisions of large nuclei at low energies, this was straightforward to understand as the reinteraction of the initial baryons and the produced hadrons, which would thermalize and evolve as a "hadron gas". However, its persistence at higher energies, particularly at RHIC where the value of v_2 averaged over $p_{\rm T}$was twice as large as it was at the CERN SPS, surprised many who expected the hot system to become more dilute and more weakly-interacting at higher energies.

Collective flow was a major piece of the RHIC program, and its characterization in terms of hydrodynamics was a crucial piece of evidence in the RHIC discovery of the strongly-coupled quark gluon plasma (sQGP). Crucial aspects of collective flow, on the experimental and theoretical sides at RHIC, have been:

- Based on theoretical calculations, the average elliptic flow, scaled by the eccentricity, is thought to reach a limiting value in the limit where the viscosity can be ignored. RHIC data achieved this limit both integrally (integrated over $p_{\rm T}$) and for $v_2(p_{\rm T})$, which rises linearly until viscous corrections become large.

- When studied as a function of particle type, it is found that heavier particles show a smaller v_2 at the same $p_{\rm T}$at low $p_{\rm T}$, while this hierarchy flips above 1.5 GeV, where protons typically have a 50% higher value of v_2. This behavior has been explained by the hadronization of the system via constituent quarks which recombine into baryons with v_2(baryon)=(3/2) $\times$ v_2(meson).

- The deviations from ideal behavior can be systematically calculated by viscous corrections, and all RHIC data point to a small but significant value of the ratio of shear viscosity to entropy density (η/s).

- While difficult to calculate in the strongly-coupled limit, where the approximations required for kinetic theory break down, AdS/CFT-based calculations have shown that a wide range of strongly-coupled systems have a lower-bound on $\eta/s = 1/4\pi$. The RHIC experimental data suggest values of 1-2 times this bound, although esimates are limited by theoretical uncertainties related to the modeling of the initial state.

- When studying smaller systems (particularly Cu+Cu), it was found that accounting for the event-by-event position of the nucleons in the nuclear wave functions showed scaling in the quantity v_2/ϵ between Cu+Cu and Au+Au, when plotted as a function of the transverse density of charged particles at mid-rapidity, estimated by $dN_{ch}/d\eta/S$, where S is the overlap area of the two nuclei.

5.2 Methods

Harmonic flow is a global modulation of essentially all of the particles in an event relative to an event plane appropriate to each harmonic. However, there are additional sources of multiparticle correlations, some which lead to global correlations (momentum conservation) and others which only lead to correlations local in angular space (e.g. resonance decays and jets). Thus, care must be taken to minimize such "non flow" correlations.

One of the earliest methods for measuring flow was the "event plane" method, which calculates an event plane using a forward detector and correlates all particles with this event plane, based on the so-called "Q-vector" for each order n:

(2)

From this, the n-th order event plane Ψ_n is simply determined as the angle of the Q-vector itself. From the definition of the Q-vector, the angle is n-fold ambiguous, but this has no effect on the extracted v_n coefficient, which is defined as

$$v_n = \frac{v_n^{obs}}{/}\mathrm{Res}\{n\Psi_n\} = \frac{\langle\cos(n[\phi - \Psi_n])\rangle}{\langle\cos(n[\Phi_n - \Psi_n])\rangle} \tag{3}$$

where Φ_n is the direction of the true event plane. The latter quantity cannot be observed directly and so the resolution parameter must be derived from comparison of different detector regions. This is typically done by comparing symmetric pseudorapidity regions separated from the region being measured:

$$\mathrm{Res}\{n\Psi_n^{\mathrm{P(N)}}\} = \langle\cos n(\Psi_n^{\mathrm{P(N)}} - \Psi_n)\rangle = \sqrt{\langle\cos n(\Psi_n^{\mathrm{P}} - \Psi_n^{\mathrm{N}})\rangle} \tag{4}$$

Non-flow contamination is typically most difficult to control when the subevents used to determine the event plane and resolution are close in η to each other or close to the measured particles. Another method is to use multiparticle cumulants to explicitly remove lower order correlations. These can be calculated either from a generating function formalism, or through moments of the Q-vector itself. They are more or less sensitive to non-flow depending on the order of the cumulant. For example, the two-particle cumulant is quite senstitive to effects from resonance decay and jet fragmentation. However, the four particle cumulants are generally much less so, since it explicitly removes short-range two particle correlations. A third method is to use the "Lee Yang zeroes" approach, which accounts for correlations of all lower orders using a different generating function. The method relates the zeros of a complex function to the magnitude of the relevant flow harmonics. While the method is thought to be robust against most sources of non-flow, it is particularly sensitive to multiplicity fluctuations, and so is calculated using event samples with similar multiplicities within a given centrality interval. Theses subsamples are then averged within the desired centrality interval to give the final result.

5.3 Elliptic flow

The first LHC data on elliptic flow was released by the ALICE collaboration soon after the first collisions, and is shown in Figure **??**. The elliptic flow was estimated using three methods: 2-particle cumulants ($v_2$2), 4-particle cumulants ($v_2$4) and Lee-Yang Zeros (LYZ). The first method is known to be sensitive to correlation from jets, which have a larger contribution at the LHC than at RHIC, and the latter method was only used for integral flow. The integral flow was found to be larger than that measured at RHIC, but only by about 15-20%. What was surprising was that, as a function of p_{T}(but only measured out to 4 GeV) the magnitude of v_2 was found to be quantitatively very similar to that measured in the STAR experiment at RHIC, using similar cumulant methods. Although a similar scaling has been observed in the very low energy data on inclusive $v_2(p_{\mathrm{T}})$ from STAR taken during the recent RHIC energy scan, there is no fundamental understanding yet of how this scaling arises. It suggests that most of the variation in the integral elliptic flow results from the change in the spectral shape of inclusive hadrons. Hydrodynamic calculations were able to reproduce this result, soon after its release, estimating a slightly higher viscosity to entropy ratio based on a scaling of the initial energy density according to the measured charged-particle multiplicity [**?**] [CHECKME]. The first v_2 measurement at higher $p_{\mathrm{T}}$was performed by ATLAS [**?**], showing the transition from the low p_{T}behavior, understood by viscous hydrodynamics, to the higher p_{T}values presumably explained by the path-length dependence of

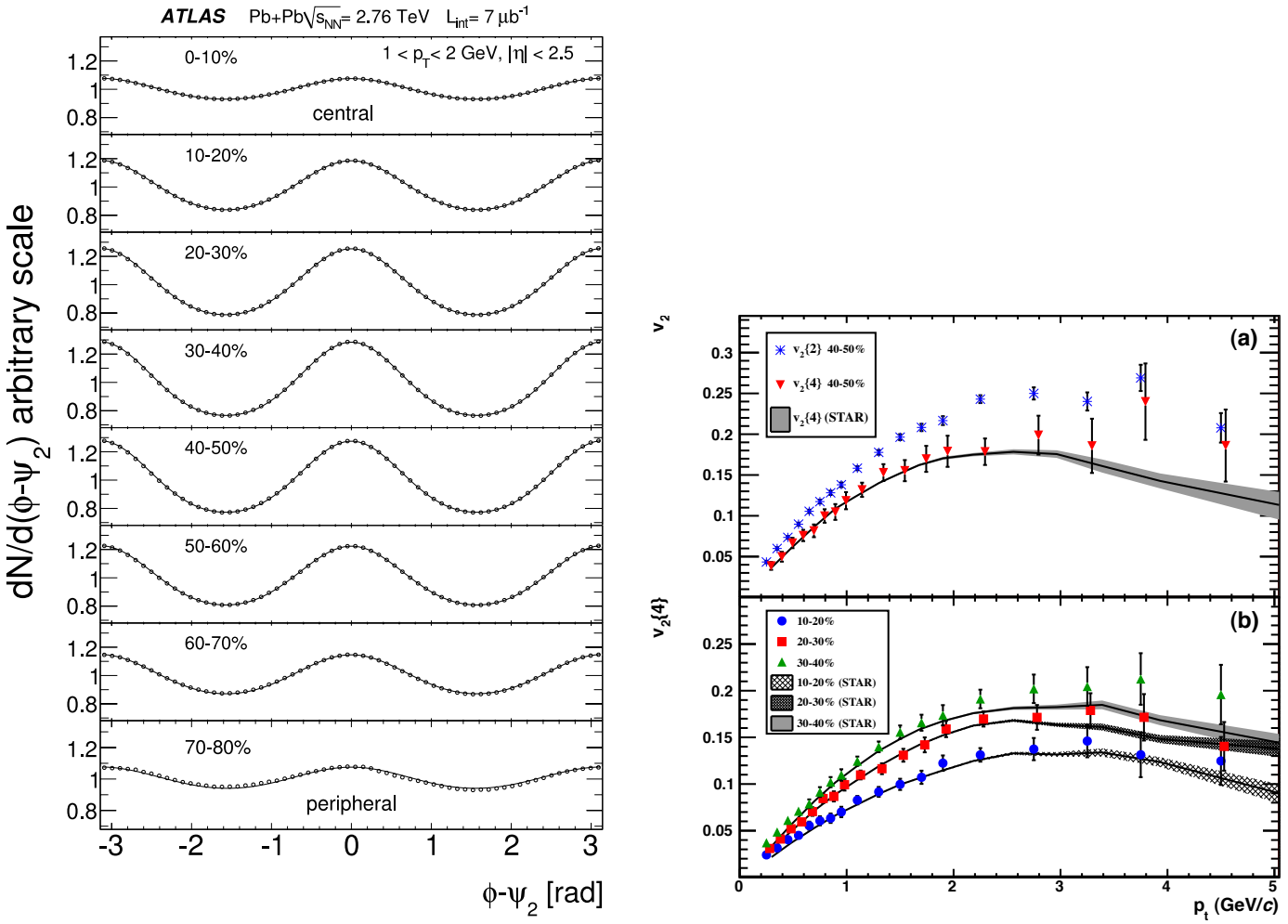

Figure 7: (left) ATLAS data showing the evolution of anisotropy relative to the reaction plane, as a function of centrality (right) First ALICE data on $v_2$in Pb+Pb collisions at the LHC.

energy loss of jets. By comparison with PHENIX data on π^0 particles, this shows that the scaling of v_2 extends to high p_{T}as well, within the large statistical errors of the lower-energy measurement.

The dependence of the inclusive elliptic flow on the initial state geometry was studied carefully by CMS, who performed a careful extrapolation of the integral v_2 down to $p_{\mathrm{T}} > 0$ GeV, using simultaneous measurements of dN/dp_{T}, to match with the lower energy PHOBOS data. To factor out the initial shape and size of the overlap region, a Monte Carlo Glauber model was used to match the centrality selections made with the CMS forward calorimeter. From these, the eccentricity and overlap area were calculated according to the definitions from subsection**??**. The CMS data, shown superimposed on data from RHIC, is shown in Figure 8(right), and overlaps the PHOBOS data in the most peripheral collisions and shows a continuous rise in the more central collisions, except perhaps in the most central interval.

The CMS data shown in Figure 9 illustrates the p_{T} and centrality dependence of $v_2(p_{\mathrm{T}})$, comparing directly the different methods of flow reconstruction used for v_2. While it is clear that the 2-particle cumulant is the most contaminated by non-flow, particularly at high p_{T}, one also observes some systematic differences between all three methods, particularly where the flow is the strongest.

The previous results have all been for unidentified hadrons. This choice provides the largest phase space coverage (particularly in p_{T}) and allows for comparisons between experiments with different particle identification capabilities. However, a study separating the different hadron species is crucial,

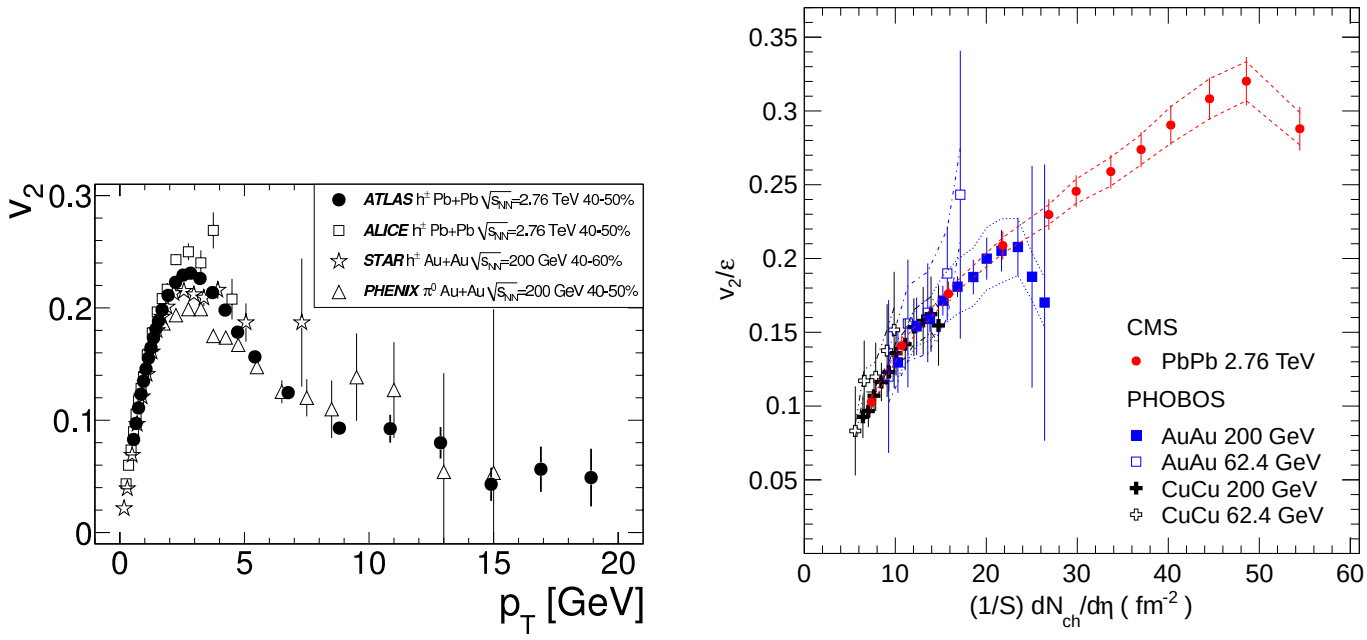

Figure 8: (left) ATLAS data showing the invariance of $v_2(p_{\mathrm{T}})$ with beam energy (right) CMS compilation showing the observed scaling of v_2/ϵ vs. $(1/S)dN_{ch}/d\eta$.

given the previous measurements at RHIC showing the strong differences between them. The ALICE data showing identified particles (separated using the dE/dx measured in the ALICE TPC) for $p_{\mathrm{T}} > 3$ GeV is shown in Figure 10(left). The charged pion data on $v_2(p_{\mathrm{T}})$ is quantitatively similar to the PHENIX π^0 data over the p_{T} range where they overlap. The proton-antiproton v_2 are found to be subsantially larger than the pion values over the measured p_{T} range, although it is clear that the peak-plateau structure seen in the inclusive hadron data is not explained primarily by one particular hadron type. Also, at the highest p_{T} measured, the protons and pions are quite close, although the protons remain systematically higher out to 14 GeV. CMS extends the hadron p_{T} range out to the full range provided by the LHC in 2011, using a high p_{T} high level track trigger. The data, shown in Figure 10(right), show that the plateau observed setting in above 6 GeV extends out to 50 GeV, with only mild decreases observed within the stated uncertainties.

Another intriguing way to compare with the lower energy data is suggested by studies performed by the PHOBOS collaboration, which found that the integrated $v_2(\eta)$ is the same for different colliding beam energies, when plotted in the rest frame of one of the projectiles. This is the phenomenon of so-called "limiting fragmentation", where many quantities are found to depend only on their rapidity relative to either beam or projectile. Figure 11 shows $v_2(\eta)$ as a function of $\eta - y_{\mathrm{beam}}$ (in the forward hemisphere) and $\eta + y_{\mathrm{beam}}$ in the backward hemisphere. While the CMS and PHOBOS data points do not overlap in any measured region, they appear to be continuous in the forward LHC kinematics and the mid-rapidity RHIC kinematics. However, it is clear that the behavior of the CMS data is much more suggestive of a boost-invariant central plateau, while the PHOBOS data did not show similar behavior.

5.4 Higher order harmonics

Although the realization that v_2 was sensitive to fluctuations in the nuclear overlap, particularly from the eventwise random positions of nucleons in each nuclei, several more years elapsed before it was suggested to look for higher-order harmonic flow, particularly odd-orders [**?**]. Many authors argued

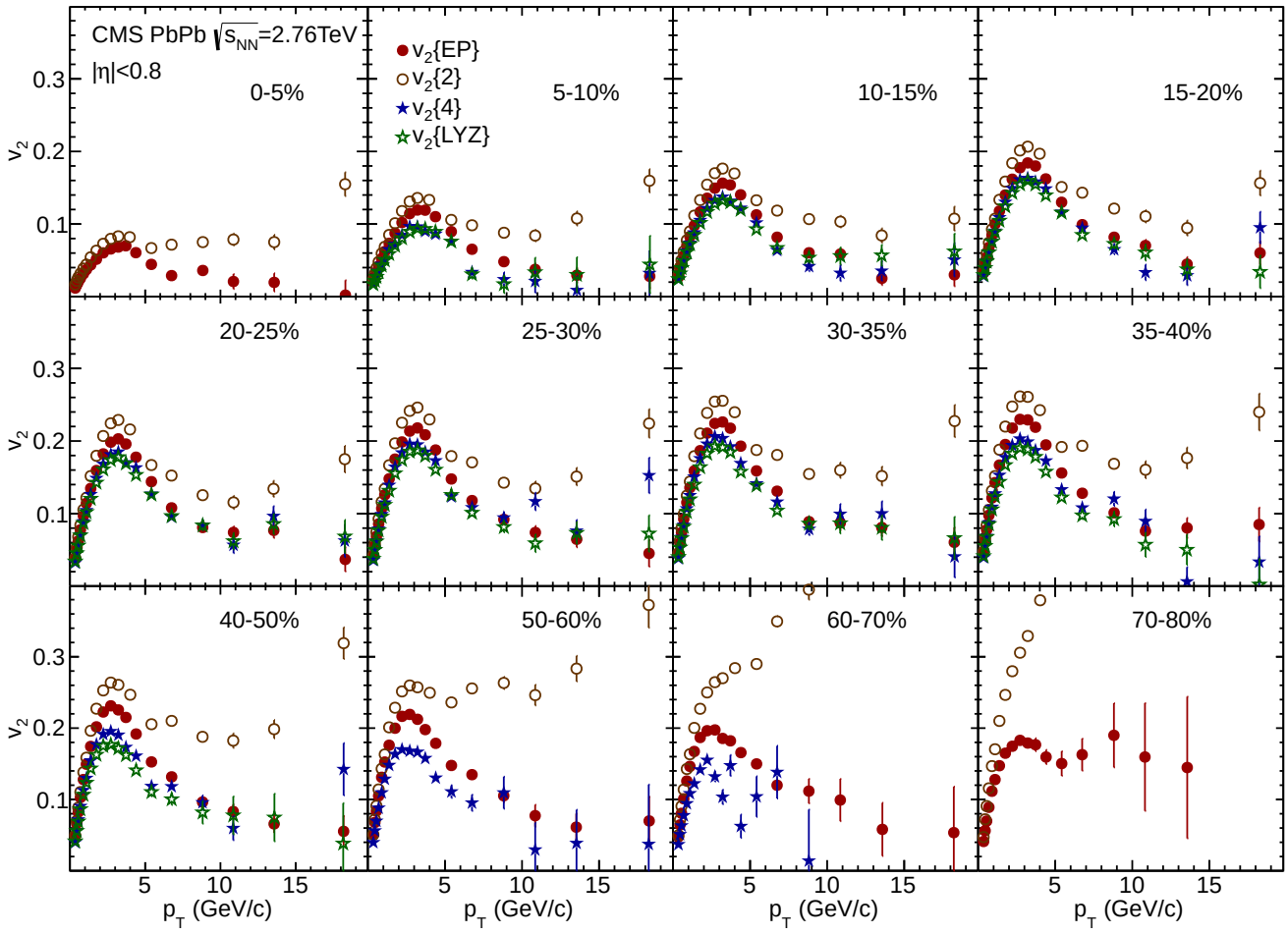

Figure 9: CMS data showing $v_2(p_{\rm T})$ in centrality intervals, using four different methods of extracting v_2: event plane (EP), 2-particle cumulants, 4-particle cumulants, and Lee-Yang Zeros.

that symmetric systems would have a zero v_1, v_3, v_5, etc, but had not yet considered the effect of fluctuations. By mid-2011, all of the LHC and RHIC experiments had significant measureents of many of the higher-order contributions, up to v_6 which was the limit of the statistics in the 2010 run.

CMS released the first evidence for the presence of higher-order harmonics in the two-particle correlation function. ALICE released the first measurements of of $v_3 - v_5$ up to $p_{\rm T} = 4$ GeV, using two and four particle cumulants [**?**], and followed up with an extensive study of two-particle correlations in Ref. [**?**]. ATLAS released the first large scale study of higher harmonics for unidentified hadrons, with the first complete experimental measurements of

The ATLAS data shown in Figure 12(left) and (right) show the harmonics $v_2 - v_6$ as a function of $p_{\rm T}$in centrality intervals from the most central 0-5% to the most peripheral 70-80%. The the figure on the left shows that the pattern is consistently the same for all harmonics: a rapid rise starting at low $p_{\rm T}$, a peak around 3 GeV, and a rapid decrease out to higher $p_{\rm T}$. While all of the experiments have demonstrated that v_2 does not necessarily go to zero at high $p_{\rm T}$, it remains an open question about the higher harmonics, which can only be resolved with higher statistics. The right figure shows the centrality dependence in small $p_{\rm T}$intervals, demonstrating that v_2 is fundamentally different than the higher harmonics, having a much milder centrality dependence. While v_2 mainly reflects the overall geometric shape of the system, the higher harmonics seem to mainly reflect fluctuations. However, the

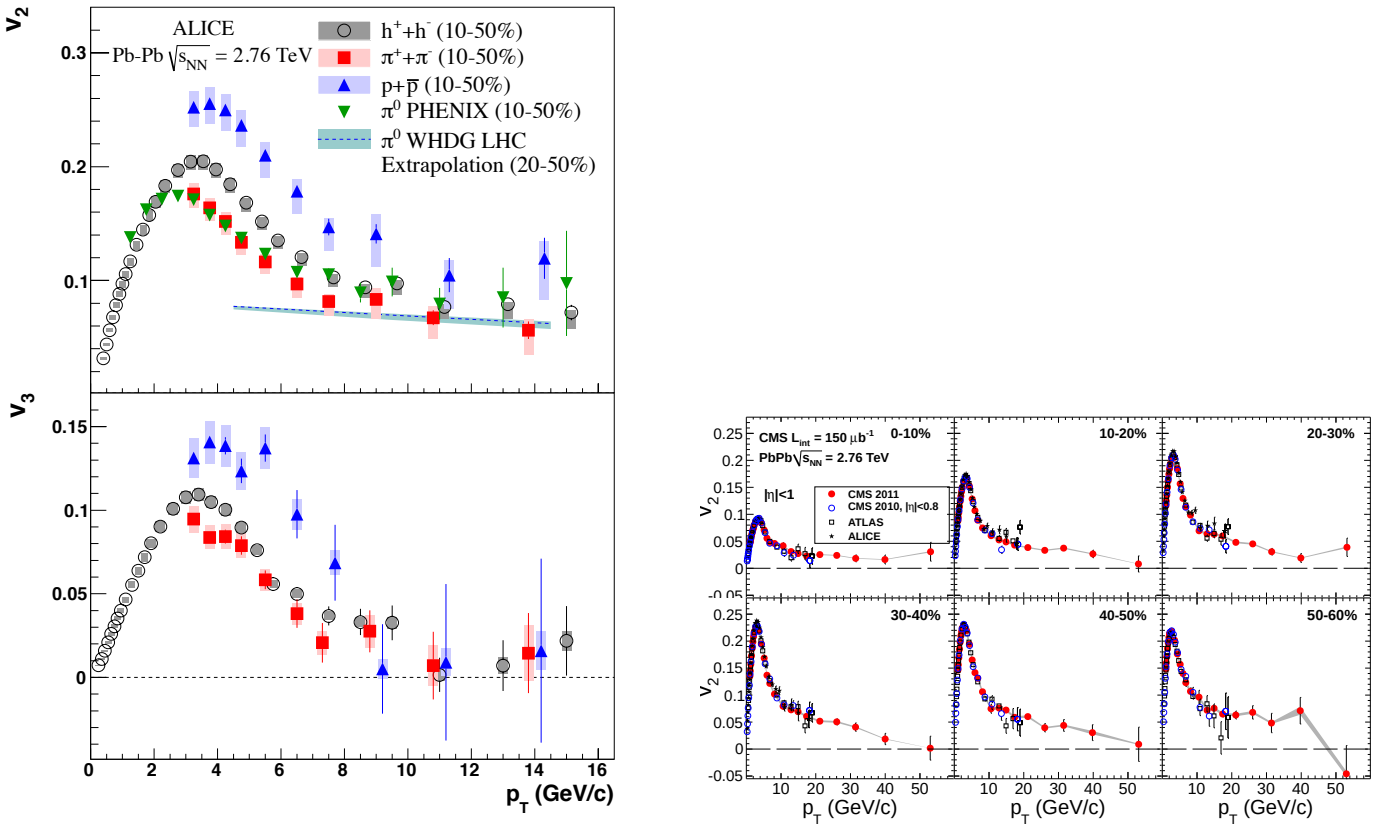

Figure 10: (left) ALICE data showing $v_2(p_{\rm T})$ for identified hadrons, for $|\eta| < 0.8$ (right) CMS data showing the v_2 for unidentified hadrons at very high $p_{\rm T}$, out to 50 GeV

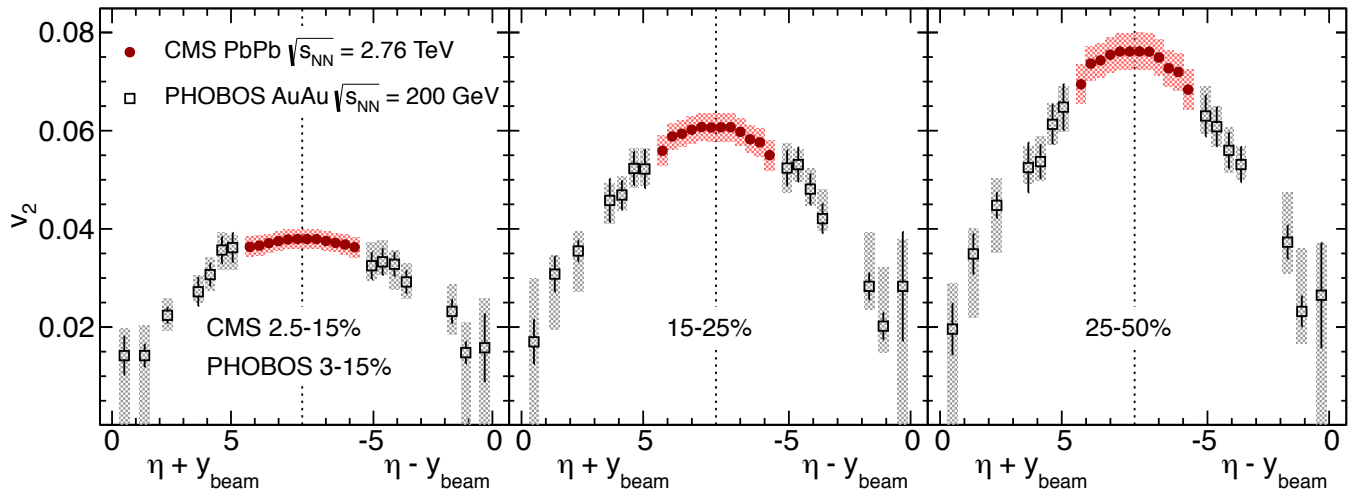

Figure 11: CMS data showing v_2 for unidentified hadrons as a function of $\eta - y_{\rm beam}$, averaged over $0 < p_{\rm T} < 3$ GeV (using an extrapolation procedure to cover $p_{\rm T} < 300$ Mev). Results are compared to data from $\sqrt{s_{NN}} = 200$ GeV at large η from the PHOBOS experiment at RHIC.

decrease in magnitude with increasing n is generally thought to reflect the presence of viscous effects.

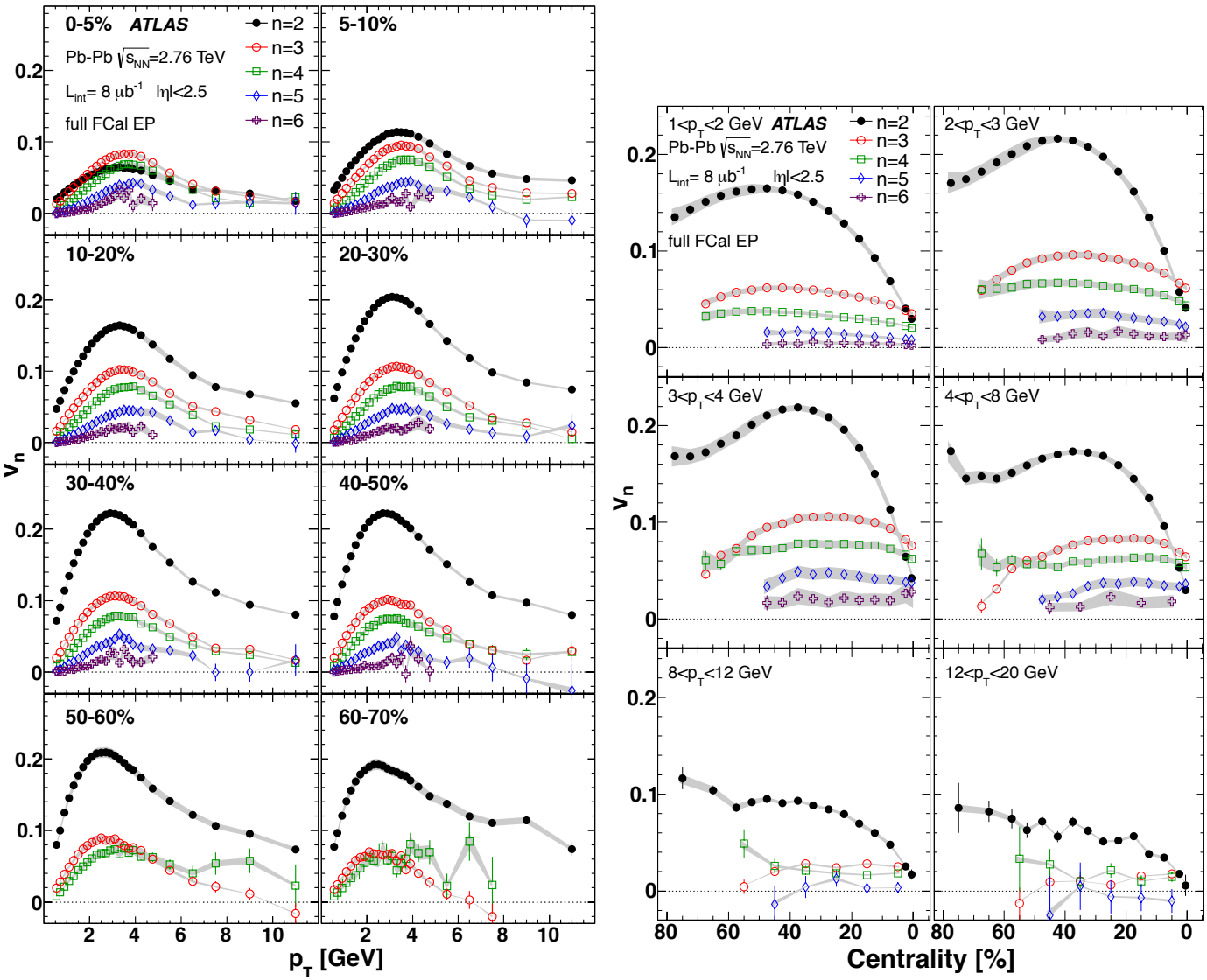

Figure 12: (left) ATLAS data showing $v_n(p_{\rm T})$ for different centrality intervals and $|\eta| < 2.5$, for $n = 2{-}6$. Very little dependence on η is observed. (right) The same ATLAS data, in $p_{\rm T}$intervals, showing the centrality dependence of v_n.

Another representation of this data is given in Figure 13, which shows the "angular power spectrum", the n dependence of $v_2(p_{\rm T})$ for particular intervals in $p_{\rm T}$and centrality. The fall-off with increasing n is a general feature, of the data which is expected to be driven by viscous corrections that increase with n.

While the two-particle analyses from ALICE, ATLAS and CMS all utilized a $v_{1,1}$ term in their fits, the first measurements did not extract a single-particle v_1 contribution, since momentum conservation is expected to be a substantial effect. The first published extraction of v_1 from experimental data was performed by a theoretical team using published ALICE data, doing a fit of the form $V_{1\Delta}(p_T^a, p_T^b) = v_1(p_T^a)v_1(p_T^b) - kp_T^a p_T^b$. ATLAS was the first experimental group to measure directed flow from its own data, using the same approach as Ref. [**?**](but performed in isolation from it), fitting $v_1(p_{\rm T})$ The value of v_1 was also found to change very little with centrality, suggesting it too arises from fluctuations.

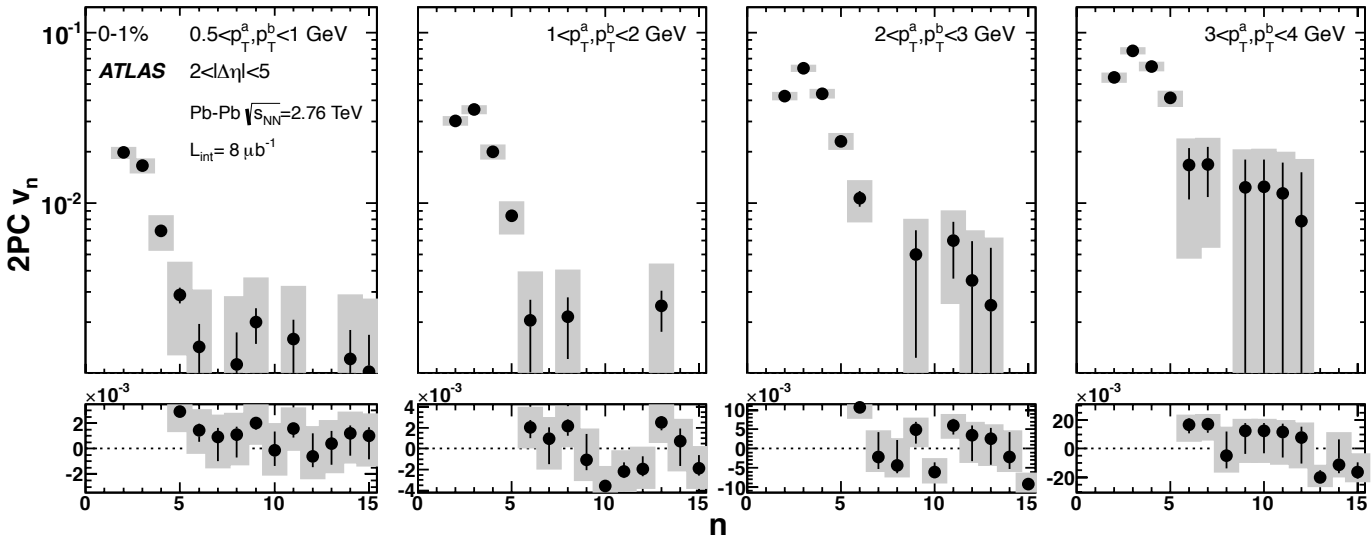

Figure 13: ATLAS data showing the n dependence of v_n in four p_{T}intervals, which are effectively angular power spectra at different resolution scales.

5.5 Flow fluctuations

The same geometric fluctuations that lead to the presence of the higher harmonics are also expected to lead to event-by-event fluctuations in the individual coefficents. This has been studied using two methods. ATLAS developed a data-driven method to unfold the measured v_n distributions ($P(v_n)$) with a Bayesian technique. The distributions $P(v_n)$ are shown in Figure 15 for v_2, v_3 and v_4 for a selected set of centrality intervals. It is clear that the fluctuations are large in all selected samples. Although the distributions are not Gaussian, but are rather projections of a 2D Gaussian (also known as a Bessel-Gaussian distribution), the distributions are typically quantified using the first two moments, the mean and standard deviation. These can also be estimated by combining different estimates of v_n, in particular using the event-plane and 4-particle cumulant methods. Based on the analysis of Ref., the difference between these quantities is twice the variance, while their sum is twice the squared mean. Figure 16(left) shows CMS data on $\sigma/\langle v_2\rangle$ derived from cumulants, compared with the ATLAS data derived from the fully unfolded distributions. While the v_2 fluctuations compare well between the two methods, the ATLAS and CMS results on v_3 are quite different, possibly from the inapplicability of the cumulant approach for this quantity. The ATLAS results are essentially constant for all centrality intervals at around 0.5, which is the value one gets ($\sqrt{4/\pi - 1}$) if the fluctuations are described by a 2D Gaussian, projected along the radial direction. Figure 15(left) shows ALICE data on $\sigma/\langle v_2\rangle$ derived using a similar approach as CMS. For centrality intervals from 5-60%, the overall magnitude is similar to that seen by the other experiments. However, this figure points out that the fluctuations have essentially no centrality dependence out to moderately large p_{T}, about 8 GeV, which reaches into the plateau region typically associated with differential energy loss.

6 Electroweak probes

While a primary topic in the study of heavy ion collisions is the modification of jets in the hot and dense nuclear medium, typical analyses of hard processes have assumed that the structure of a nucleon in a nucleus-nucleus collision is quantitatively the same as one in a nucleon-nucleon collision. From analyses of lepton-nucleus deep inelastic scattering data, it is known that cross sections do not scale linearly with

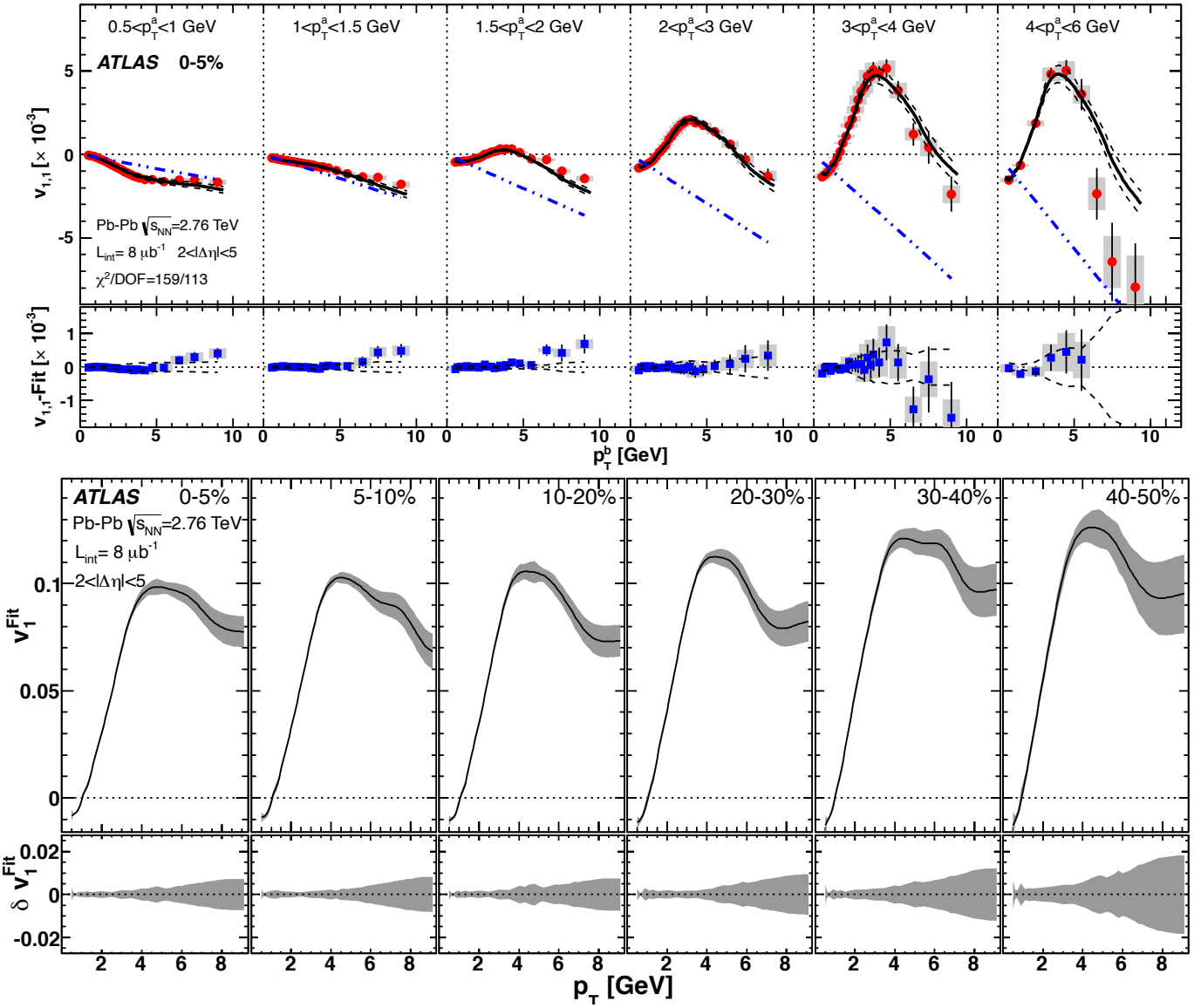

Figure 14: (top) ATLAS data showing the amplitude of $v_{1,1}$ the dipole modulation in the 2-particle correlation function, as a function of p_T^b for ranges in p_T^a. The fit used to extract the functional form of $v_1(p_{\rm T})$ is shown. (bottom) The extracted functional form of $v_1(p_{\rm T})$, from the fits shown above, as a function of centrality.

the number of nucleons, as might be expected simply from the availability of scattering centers. The deviations from this scaling are referred to generally as "nuclear shadowing", and are typically shown as a function of Bjorken x for different ranges in the hardness scale Q^2. The region around $x \sim 0.1$ corresponds to the valence quark region for a standard nucleon, and this is usually enhanced. The region above this, $x \geq 0.2$ is typically suppressed (the so-called "EMC effect"), while the region below $x << 0.1$ is also suppressed down to very small values of x. The latter phenomenon is more typically known as "nuclear shadowing" and is thought to arise generally from quantum mechanical effects which deplete the numbers with small fractions of the nucleon momentum.

It is of clear urgency to understand the magnitude of these sorts of effects in the realistic environment of a heavy ion collision, in order to properly interpret measurements of hard process rates relative to a nucleon-nucleon reference system. At the RHIC collider, this was addressed early in the experimental program through measurements of high $p_{\rm T}$ particles in deuteron-gold collisions. Presumably, any gross

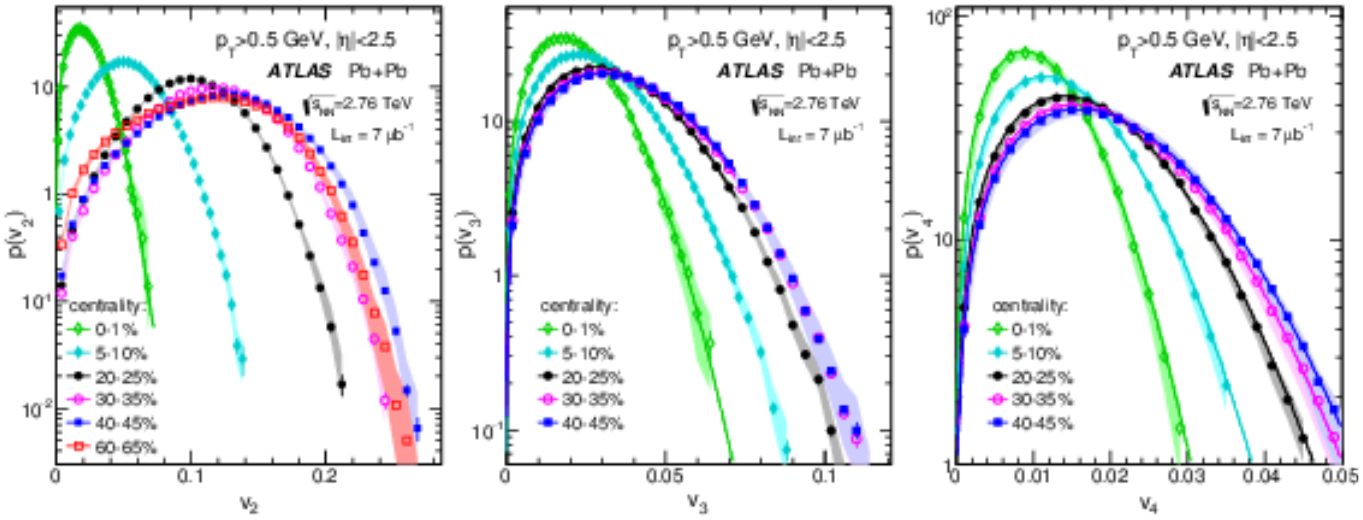

Figure 15: ATLAS data on the event-wise distributions of the harmonic coefficients $v_2 - v_4$ presented in a selection of centrality intervals.

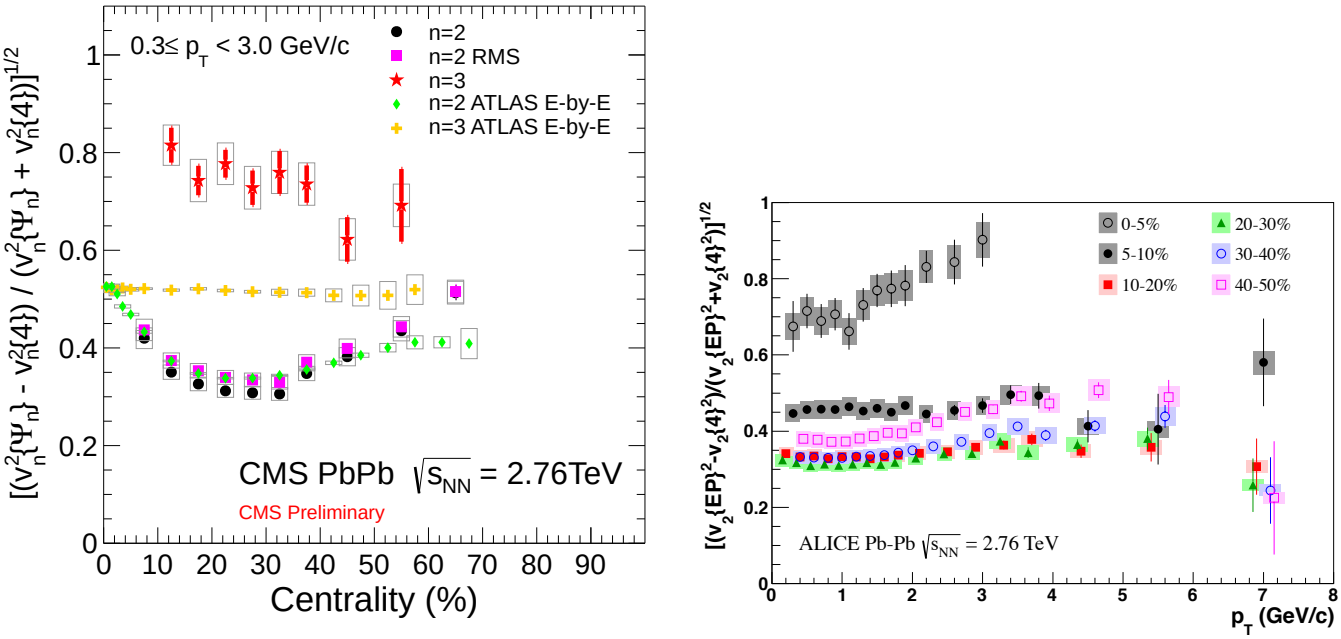

Figure 16: CMS data on the centrality dependence of the standard deviation of v_2 divided by the mean, for $0.3 < p_{\rm T} < 3$ GeV, extracted via the differences between the EP and cumulant results. ALICE data on the $p_{\rm T}$ dependence of the same quantity, out to $p_{\rm T} = 8$ GeV, for a selected set of centrality intervals.

effects related to modifications of nucleon structure in the nuclear environment would show up as modifications in this system. It was found that hadrons above ~ 2 GeV were produced at expected rates near $\eta = 0$, confirming that the high $p_{\rm T}$ suppression observed in the early days of the RHIC program did not arise from changes in nucleon structure, and strengthening the case for jet suppression in the hot and dense medium. However, it was also found that hadrons and J/ψ particles were suppressed at forward angles, in the direction of the incoming deuteron, especially in more "central" d+Au collisions, and enhanced slightly at backwards angles, in the direction of the nucleus. These features are in

broad agreement with predictions from calculations incorporating the nuclear shadowing observed in lepton-nucleus DIS.

While the measurement of hadronic final states in proton (or deuteron)-nucleus collisions is thought to give useful information on modifications in the initial state of these simpler systems, the abovementioned observed modifications of jets precludes similar observables giving similar information in heavy ion collisions. For this reason, great attention has been given to the measurement of "penetrating probes", particles which do not interact strongly after they are produced. While charged leptons and neutral photons, of course, do not interact strongly, they come predominantly from jets and hadrons at relative low $p_{\mathrm{T}} < 20$ GeV. However, at high p_{T}, most leptons are known to arise from the decay of electroweak bosons (Z and W particles). Furthermore, isolated photons at high p_{T} are predominantly "prompt", i.e. arising from the direct interactions of quarks and gluons and not from electromagnetic decays of hadrons (π^0 and η).

While the production cross sections for the heavy bosons are prohibitively small at the top RHIC energies (200 GeV per nucleon-nucleon collision), the LHC provides the first heavy ion system where all of the electroweak bosons are produced at substantial rates. This section presents measurements of all three particles in Pb+Pb collisions at the LHC, and shows their comparisons either with nucleon-nucleon reference data, or cross sections calculated with perturbative QCD using standard structure functions. The main physics goals of these measurements are twofold

- To establish whether the production of the vector bosons is proportional to the nuclear thickness or, equivalently, the number of binary nucleon-nucleon collisions

- To see whether any modifications of vector boson production can be observed, and if they can be attributed to modifications of the nuclear PDFs

Theoretical calculations provide some guidance as to the magnitude of the modifications of standard PDFs expected in nPDFs, but substantial uncertainties remain due to the different parametrizations of the existing nDIS data. One feature which is predicted generically, however, is the decreasing magnitude of nuclear modifications with increasing Q^2. As shown in Fig.**??**, the large magnitude of shadowing expected at low Q^2 (i.e. low p_{T}) is reduced substantially even by $Q^2 = 100$ GeV. Considering that M_Z and M_W are 80-90 GeV, it is no surprise to find that nuclear modifications are expected to be at the 10-15% level.

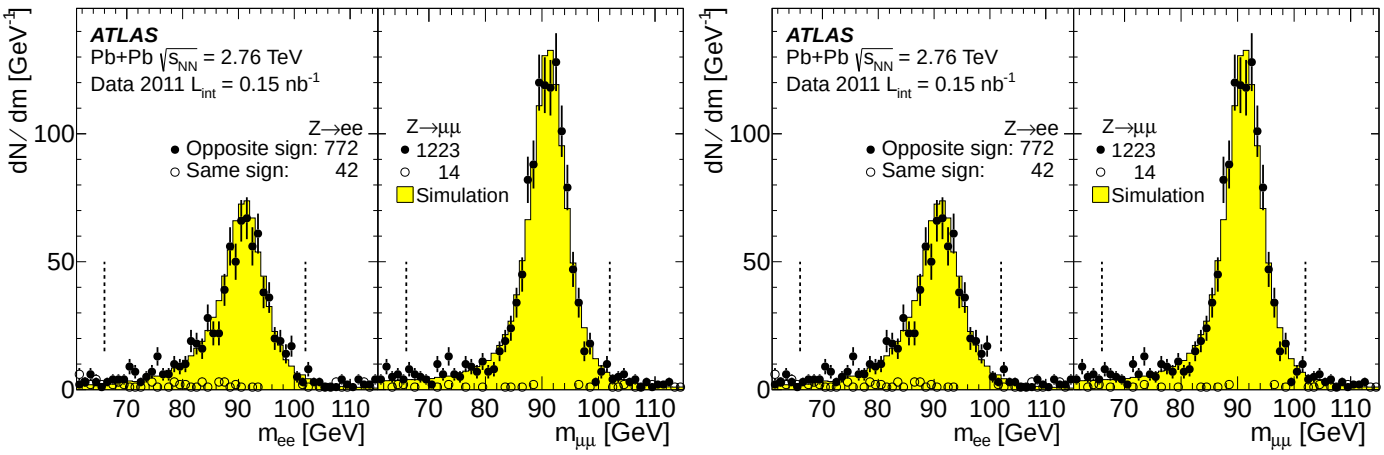

Figure 17: (left) Single muon spectrum, after selection cuts (right) Dimuon mass spectrum, in electron and muon channels.

6.1 Measurements of W and Z bosons in Pb+Pb collisions

The first observation of vector bosons in Pb+Pb collision was performed by the ATLAS experiment with a set of 38 Z candidates obtained in the first heavy ion run in 2010, which was followed several months later by a CMS result comparing with theoretical calculations. However, the statistical power of the 2010 sample was not sufficient to make strong conclusions about the Z production rates as a function of the nuclear thickness. The situation has improved dramatically with a published measurement of W bosons by CMS, also from the 2010 dataset, but benefiting from the large increase in the W cross section compared with Z. ATLAS has also published the yield and spectrum of Z bosons from the much larger 2011 Pb+Pb dataset. Together these give a relatively complete first look at the behavior of heavy vector bosons in heavy ion collisions.

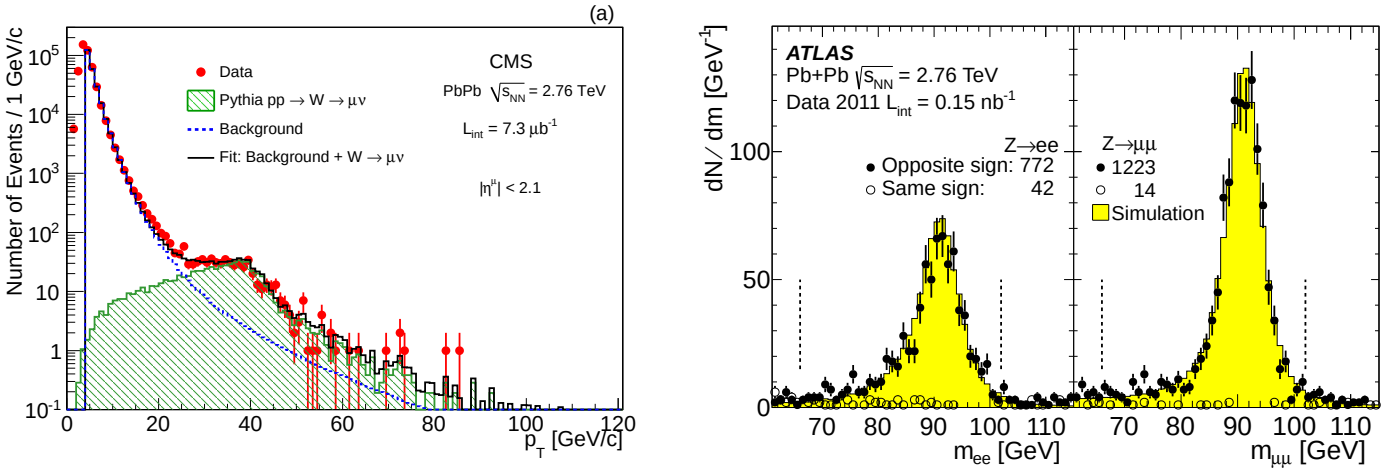

Figure 18: (left) Single muon spectrum, after selection cuts, from CMS data (right) Dimuon mass spectrum, in electron and muon channels from ATLAS data.

The CMS W measurement was performed using the CMS inner tracker, which covers $|\eta| < 2.4$ and the CMS muon spectrometer, which covers $|\eta| < 2.4$ using a variety of gaseous detectors (CSC, DT, with RPCs used for triggering), but was restricted to $|\eta| < 2.1$ in this particular analysis. The ATLAS Z measurement was performed combining dilepton decays in the muon and electron channels. The ATLAS muon spectrometer uses drift tubes and cathode strip chambers to measure muons with $|\eta| < 2.7$ in tandem with the ATLAS inner detector covering $|\eta| < 2.5$. Electrons are measured in ATLAS using the inner detector in association with the ATLAS calorimeter system, which is particularly finely segmented in η for $|\eta| < 2.5$, allowing rejection of jet backgrounds.

As shown in Figure 18(left) from CMS, the single muon spectrum at high p_{T} clearly shows a contribution from W bosons as a peak near 40 GeV. The backgrounds from jets are strongly reduced by calculating the missing p_{T} for each event with a high p_{T}muon, based on tracks with $p_{\mathrm{T}} > 3$ GeV. The background from Z bosons is removed by removing muons which combine with a second muon in the same event that reconstructs to a mass near the Z mass. After selections, about 540 W candidates were found in the 2010 Pb+Pb data. Figure 18(right) shows the dimuon and dielectron mass spectrum after requiring $p_{\mathrm{T}} > 10$ GeV for the muons, and $p_{\mathrm{T}} > 20$ GeV for the electrons. The Z lineshape is in good agreement with simulations for both dielectron and dimuon channels. After selections, about 2000 Z candidates were reconstructed in the 2011 Pb+Pb data.

Figure 19(left) shows the pseudorapidity dependence of the charged lepton asymmetry for the muons associated with W candidates ($A_\mu = (N_{W^+} - N_{W^-})/(N_{W^+} + N_{W^-})$), both for Pb+Pb and p+p data at the same CM energy ($\sqrt{s_{\mathrm{NN}}} = 2.76$ TeV). The evident differences between the Pb+Pb and p+p stem primarily from the neutrons in the Pb nuclei, which modify the expected charge distribution,

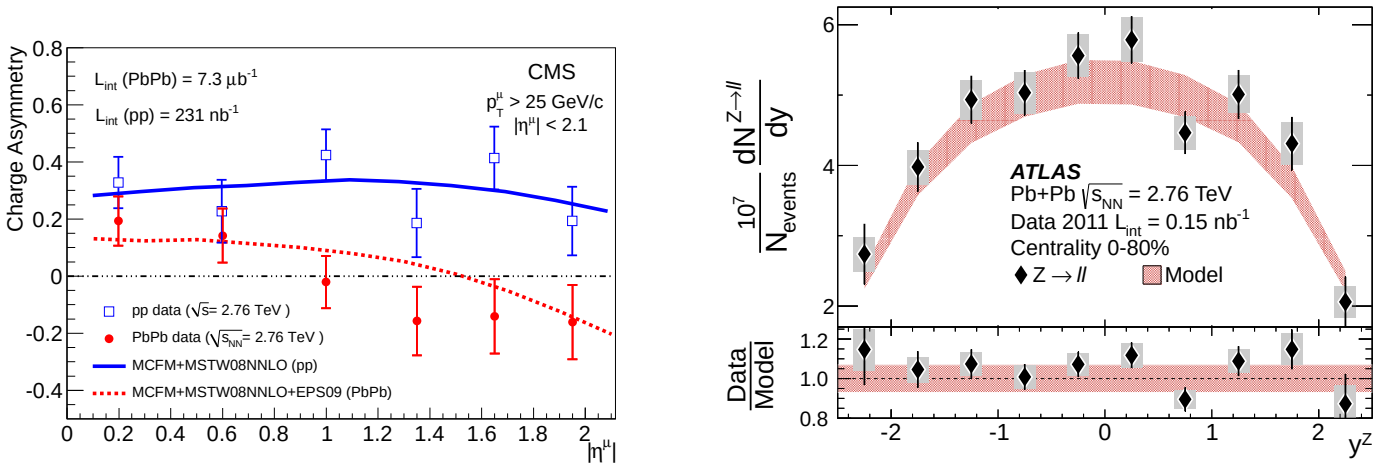

Figure 19: (left) Charge asymmetry for W candidates, from CMS data (right) Dimuon mass spectrum, in electron and muon channels from ATLAS data.

particularly in the forward direction where the Bjorken x probed is sensitive to the valence quarks. Both data sets are compared with NNLO calculations of the W charge asymmetry and good agreement is found for both p+p and Pb+Pb. While this suggests that no large nPDF effects are needed to accomodate the existing data, it was pointed out in Ref. **??** that the scale factors in EPS09 formalism will cancel out in the charge asymmetry ratio, making this quantity suboptimal for isolating nPDF modifications.

Figure 19(right) shows the rapidity dependence of the per-event Z boson yield in the 0-80% centrality interval in Pb+Pb collisions from the 2011 ATLAS Pb+Pb data. The data is compared to the same distribution from PYTHIA (version 6.425), scaled to the NNLO total cross section, and the appropriate mean nuclear thickness. Good agreement is found between the heavy ion data and the absolutely-scaled PYTHIA reference, the ratio between them being consistent with unity within the stated uncertainties. While small effects at the 10-15% level are not ruled out, nor are they required to make sense of the current measurements.

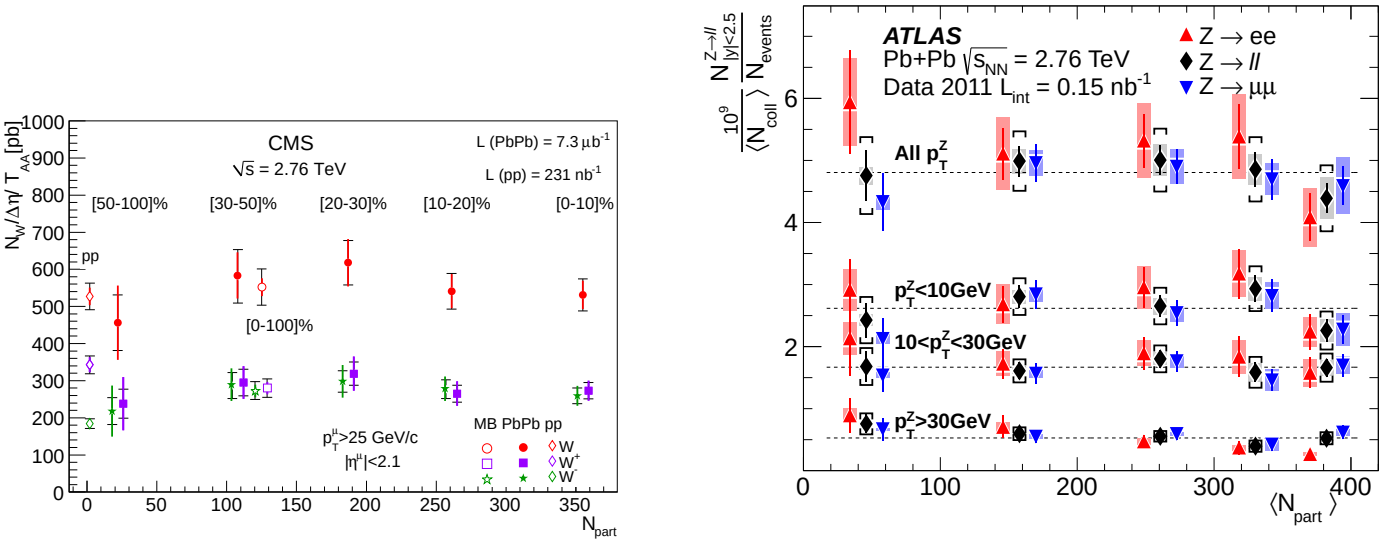

Figure 20: (left) Yield per collision for W candidates, from CMS data (right) Yield per collision for Z's, in both electron and muon channels from ATLAS data.

The centrality dependence of the separate W charge states and the total from CMS is shown in (left), as a function of the number of participating nucleons, and for the p+p data. While p+p shows a clear difference between positive and negative W's, reflecting the charges of the initial protons, there is little difference between them in the Pb+Pb data, reflecting the additional down quarks introduced via the neutrons in the Pb nuclei. The heavy ion data shows a clear scaling with centrality, once the W yields – both for the charge-separated yields, and the total – are scaled by the number of binary collisions. A similar message is found in the ATLAS Z data, shown in (right), which shows the Z yield, scaled by the number of binary collisions, also as a function of the number of the mean number of participating nucleons for each centrality interval. The ATLAS data also shows that the centrality dependence is the same for the dielectron and dimuon channels, and even for selected intervals in the Z p_{T}.

6.2 Measurement of isolated photons in Pb+Pb collisions

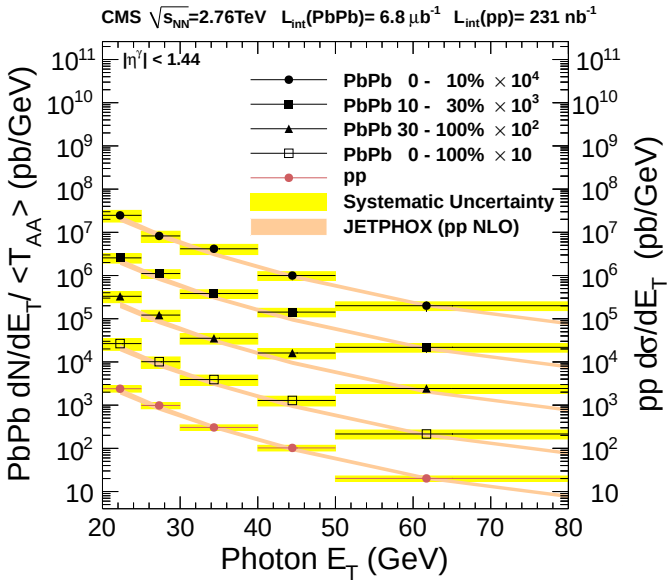

Figure 21: (left) Photon yields scaled by the mean nuclear thickness function for $|\eta| < 1.44$, from CMS data (right) The similar quantity from ATLAS, for $|\eta| < 1.3$, from ATLAS data.

The measurement of photons in heavy ion collisions is also an important contribution to the study of the Pb+Pb initial state, with some advantages and disadvantages. Unlike Z and W bosons, no energy from the initial 2-to-2 scattering process is used in the boson mass, and so the cross sections at high $p_{\mathrm{T}}$are substantially higher at the same transverse momentum. However, photon measurements do not provide a clear mass peak, and nor are they associated with a track measured in an inner tracker. This means that backgrounds are an irreducible part of the measurement, particularly at low p_{T}, where one expects large contribution from jet fragmentation into high momentum neutral pions or eta mesons.

Two primary techniques are used to increase the purity of the photon sample, which is typically $O(0.1\%)$ based on the expected relative yields of photons and jets. The first is to select photon candidates as electromagnetic clusters which pass a set of selection criteria, trained on photon simulations to efficiently reject electromagnetic decays while keeping most of the produced photons. These criteria involve both the "shape" of the cluster (since photon showers are typically quite narrow), as well as the presence of energy in the "hadronic" section of the experimental caloriemters (since photon showers should typically be well-contained in the front electromagnetic sections). The second technique is to require that the photon candidate is "isolated", i.e. only a limited amount of ambient energy, including

both electromagnetic and hadronic contributions, is allowed to be present near the photon. In the context of a heavy ion collision, where there is typically a substantial amount of uncorrelated energy present, techniques must be applied to estimate and remove this energy event by event. However, even after doing this, one must account for real photons with an upward fluctuation of ambient energy nearby ("leakage") as well as fake photons with a downward fluctuation, passing the nominal selection criteria. Thus, shower-shape discriminators are typically combined with an isolation requirement, and various means exist to combine this information to estimate the true purity of a photon sample in a data-driven fashion.

The CMS photon measurement is performed using electromagnetic clusters in the CMS ECAL, with the CMS tracks and HCAL used to tag backgrounds from electrons or hadronic decays. The signal from prompt isolated photons is extracted using a two-component template fit to the distribution of $\sigma_{\eta\eta}$, a variable which reflects the width of the cluster in the η direction. The signal is derived from PYTHIA γ+jet events, embedded into real Pb+Pb data events. The background distribution is derived from a set of photon candidates which are required to fail the isolation selection.

7 Jet quenching

This is a test. test test test

8 Heavy-flavour production

Measurement of charm and beauty production plays a special role in heavy-ion physics: it provides a calibrated probe, as the input p_{T} spectra are calculable from perturbative QCD and measurable in pp collisions. In addition, this probe is conserved from its production at early stage of the collision until it escapes from interaction region, and is eventually detected. This enables a direct access to its interactions in the QGP, including the low- and intermediate-p_{T} regime. Two observables are studied:

- transverse momentum dependence of the nuclear modification factor R_{AA} for charm and beauty paricles;
- azimuthal-flow anisotropy of charm and beauty particles, measured as the elliptic-flow coefficient v_2.

These two topics are closely connected: the in-medium heavy-quark energy loss lowers the momenta of heavy quarks, they may then thermalize in the system, and thus participate in the collective-flow dynamics. The simultaneous measurement of the two quantities opens the possibility of the determination of the heavy-flavour transport coefficients.

Two methods are exploited to detect heavy-flavour particles. Reconstruction of invariant mass of exclusive particle decays in a secondary vertex, displaced from the interaction one, is the primary tool. A second method uses the lepton ($\mu^{\pm}$ or $\mathrm{e}^{\pm}$) p_{T} spectra to infer the heavy-flavour spectra, presuming that the leptons are produced in semi-leptonic decays of heavy-flavour particles. This way, however, a (p_{T}-dependent) mixture of charm and beauty is measured. Sometimes a requirement that the lepton is not coming from the interaction vertex is used, which helps to eliminate the background, especially at lower p_{T} (below 4 GeV). The B-meson production is also accessible with the inclusive decay $\mathrm{B} \to \mathrm{J}/\psi + X$, using J/ψ decays separated from the interaction point.

8.1 Heavy-flavour particle spectra

The p_{T} spectra of heavy-flavour particles are measured at the LHC in pp and Pb–Pb (and p–Pb) collisions. The pp results are compared to perturbative QCD calculations and other models, giving

information about preferred values for parameters, such as renormalization and factorization scales. The charm-particle spectra are measured down to very low $p_{\rm T}$ (down to 1 GeV in pp) allowing for precise determination of the total charm cross section at LHC energies. The pp spectra also serve as a normalization for Pb–Pb measurements.

In general, the heavy-flavour spectra in heavy-ion collisions are expected to be also suppressed with respect to those in pp interactions, due to the energy quenching of heavy quark when traversing the dense medium. However, the energy loss of heavy quarks is predicted to be different than that of light quarks. For the energy loss by bremsstrahlung radiation, the quark energy loss will be mass dependent. The radiation is suppressed in directions close to that of the quark, for angles below $\Theta_0 \approx m/E = 1/\gamma$, due to a destructive interference (m, E, and γ being the quark mass, energy, and gamma-factor, respectively). The heavier the quark, the larger the exclusion region (i.e. Θ_0, at a given momentum), resulting in smaller energy loss for heavy quarks compared to the light ones. This is the so called dead-cone effect introduced for the vacuum radiation [] and later applied to the medium-induced radiation in a similar way []. The predicted mass hierarchy is pronounced at $p_{\rm T}$ comparable with quark masses, and goes progressively away at very high $p_{\rm T}$. Recent model calculations include both the radiation and collisional energy loss, which results in larger suppression of heavy quarks, and gets values closer to the expectation for light ones.

There are other effects that modify the expected suppression pattern. At the LHC energies, the light-flavour particles at $p_{\rm T} \sim \mathcal{O}(10)$ GeV are mostly produced in gluon fragmentation, contrary to heavy-flavour ones produced by fragmentation of the corresponding heavy quarks. Gluons have larger colour charge than quarks by a factor 9/4, consequently a gluon has to suffer more energy loss than a quark. This colour-charge effect is reinforcing the expected difference in suppression between the light- and heavy-flavour particles. Further effects of less importance, taken into account in various models, are nuclear modification of structure functions and harder fragmentation function of heavy quarks compared to the light sector.

Charm mesons are identified in the following decay modes: $\rm D^0 \to K^-\pi^+$, $\rm D^+ \to K^-\pi^+\pi^+$, and $\rm D^{*+} \to D^0\pi^+$ (and their antiparticles), requiring the decay vertex to be displaced from the interaction point. The yields of D mesons are corrected for the feed-down from beauty decays, obtained with model simulations. This contamination amounts to 5–15 % of the yields, depending on $p_{\rm T}$ and the particle type. The $p_{\rm T}$ spectra are measured both in pp [] and Pb–Pb [] collisions, and used to construct the nuclear modification factor $R_{\rm AA}$. The $p_{\rm T}$ dependencies of $R_{\rm AA}$ for three studied D-mesons are, as expected, compatible. Therefore, the results are combined into an average D-meson $R_{\rm AA}$ according their statistics, dominated by the $\rm D^0$. Figure 22 compares the average D-meson $R_{\rm AA}$ as a function of $p_{\rm T}$ in central Pb–Pb collisions, with that of charged particles. The D-meson $R_{\rm AA}$ is perhaps a little bit above the charged-particle one, hinting at less suppression for charm quark, but the difference, if any, is very small. This tendency was recently confirmed with higher statistics charm measurements. The model calculations overlayed on data in Fig. 22 are (I) [**?**, **?**], (II) [**?**], (III) [**?**], (IV) [**?**, **?**], (V) [**?**, **?**], (VI) [**?**], (VII) [**?**], and (VIII) [**?**]. The various models show varying degrees of agreement with the charm results, and in general the inclusion of collisional energy loss improves the description. In model (I) the agreement is obtained by introducing in-medium dissociation of D mesons, in addition to radiative energy loss. The remaining models, which compute also the charge-particle $R_{\rm AA}$, have not reached good description for both cases, albeit some being not far.

Recently the family of measured D mesons was enlarged with the study of $\rm D_s^+ \to K^+K^-\pi^+$ decay. As a consequence of strangeness enhancement in heavy-ion collisions discussed in Sec. 3.3, the presence of strange quark may lead to a relative increase of $\rm D_s$ production with respect to other D-mesons. Reported preliminary results show the $\rm D_s$ $R_{\rm AA}$ in $p_{\rm T}$ region 4–12 GeV above the D-meson $R_{\rm AA}$, however, still within large uncertainties.

The behaviour of the charm-meson $R_{\rm AA}$ was confirmed by the measurement of the muon spectrum in the forward region $2.5 < y < 4$. The contribution from pion and kaon decays is subtracted from

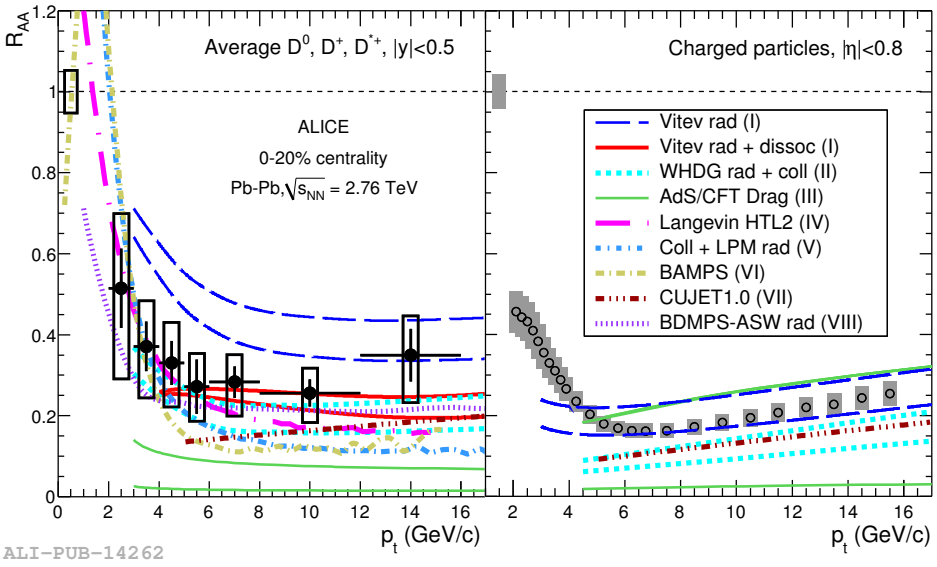

Figure 22: Average D-meson $R_{\rm AA}$ (left) and charged particle $R_{\rm AA}$ (right) as a function of $p_{\rm T}$ for the centrality between 0–20 %. The normalization uncertainties shown at unity in abscissa are almost fully correlated. The curves represent various model calculations, referred in the text, in some cases depicted as a range. Reproduced from [].

the measured muon spectrum, and the results are presented for $p_{\rm T} > 4$ GeV, where this background contribution falls below 10 %. The obtained muon $p_{\rm T}$ spectrum thus represents a mixture of muons from semi-leptonic charm and beauty decays, presumably still dominated by charm at the lowest $p_{\rm T}$ and progressively becoming beauty dominated for $p_{\rm T} > 6$ GeV. An analogous analysis of pp data is used for normalization, and the resulting heavy-flavour muon $R_{\rm AA}$ is presented in Fig. 23. The muon $p_{\rm T}$, being correlated with the heavy-flavour-particle $p_{\rm T}$, is systematically smaller than the latter one (for $p_{\rm T}$ above a few GeV). Still, the comparison with the D-meson $R_{\rm AA}$ shows qualitative agreement, since the $p_{\rm T}$ dependence is rather flat. A similar measurement using electrons in mid-rapidity region was also reported [**?**].

In Fig. 23 the preliminary CMS result for $R_{\rm AA}$ from the measurement of non-prompt J/ψ is shown [**?**]. The non-prompt J/ψ particles are selected with careful analysis of the position of the J/ψ-decay point with respect to interaction vertex. These J/ψ's are practically exclusively coming from B-meson decays. Recently reported detailed higher-statistics results on the centrality dependence of the $R_{\rm AA}$ for non-prompt J/ψ [**?**] (in $p_{\rm T}$ range 6.5–30 GeV) in comparison with the ALICE D-meson data (in $p_{\rm T}$ range 8–16 GeV) demonstrate clearly the larger $R_{\rm AA}$ for the beauty production than for the charm production, except for peripheral collisions, where the measurements are within their uncertainties. The shift between the $p_{\rm T}$ ranges takes into account that the J/ψ momentum is lowered in the decay. This is for the first time that, as expected, the energy loss for beauty smaller than that for charm is experimentally observed.

8.2 Heavy-flavour elliptic flow

The elliptic flow of charm was studied for D mesons using the event-plane method by the ALICE collaboration. To estimate the azimuthal position of the event plane charged tracks detected in the TPC are exploited. Then the yields of different D mesons are measured in the four azimuthal quadrants defined with respect to the event plane. From the yields in the two in-plane quadrants and the two out-of-plane quadrants the elliptic-flow coefficient v_2 is calculated. This is done independently for the three

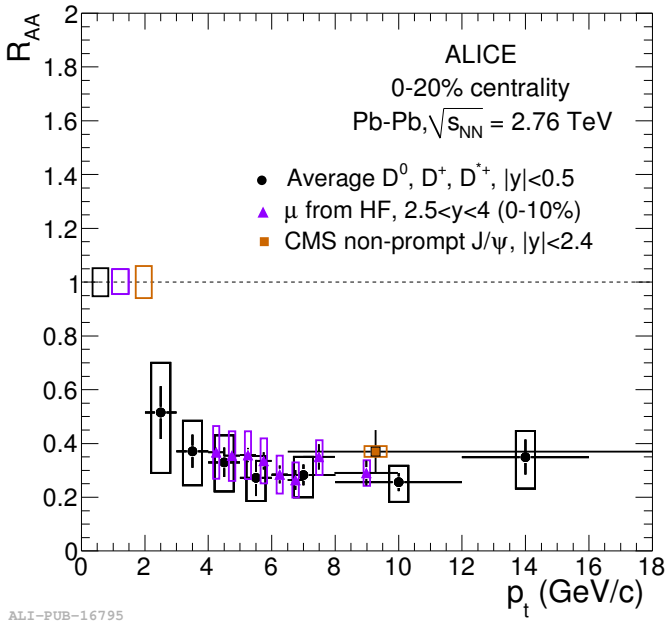

Figure 23: Heavy-flavour muon $R_{\rm AA}$ as a function of $p_{\rm T}$ compared to the average D-meson $R_{\rm AA}$. Results are for 0–20 % centrality class of Pb–Pb collisions. CMS preliminary result for beauty $R_{\rm AA}$ from measurement of non-prompt J/ψ is shown with square. Reproduced from [].

mesons: $\rm D^0$, $\rm D^+$, and $\rm D^{*+}$, and, as the v_2 values are compatible, they are averaged applying beforehand the freed-down correction as in the case of the D-meson $R_{\rm AA}$. The v_2 results for the average D meson are presented in Fig. 24 for the centrality between 30–50 %. The comparison with the charged-particle v_2 obtained with the same method reveal a similar behaviour, the v_2 values for $p_{\rm T}$ between 2–8 GeV are compatible, signaling possible in-medium thermalization of charm quarks.

9 Quarkonium production

10 Summary and outlook

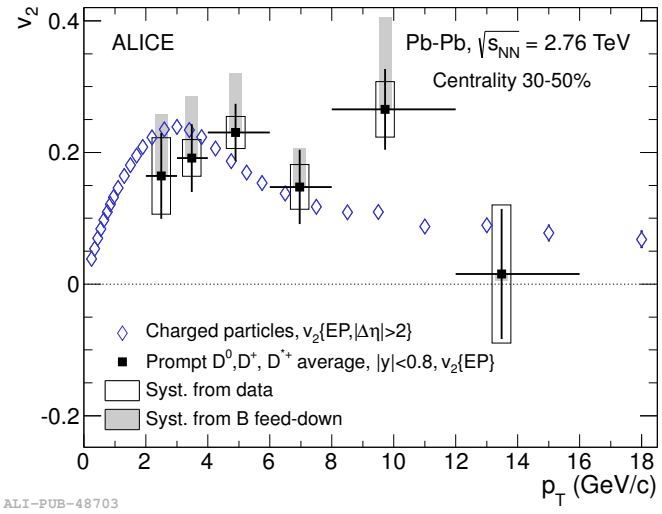

Figure 24: Elliptic-flow coefficient v_2 obtained with the event-plane method, as a function of p_{T} for the centrality between 30–50 %, averaged for D^0, D^+, and D^{*+}, compared to the charged-particle measurement. Reproduced from [].